EcoMat

WILEY

EcoMat
FUNCTIONAL MATERIALS FOR GREEN ENERGY AND ENVIRONMENT

REVIEW OPEN ACCESS

Engineering Photocatalytic Interfaces for the Inactivation of Antibiotic Resistance Bacteria and Genes

Rajendra Singh[1] | Jin Chul Joo[2] | Keugtae Kim[1]

[1]Department of Convergent Environmental Science, Dongguk University, Goyang, Gyeonggi-do, Republic of Korea | [2]Department of Civil and Environmental Engineering, Hanbat National University, Daejeon, Republic of Korea

Correspondence: Jin Chul Joo (jincjoo@hanbat.ac.kr) | Keugtae Kim (kkt38@dongguk.edu)

Received: 20 March 2026 | **Revised:** 30 May 2026 | **Accepted:** 25 June 2026

Keywords: antibiotic resistance genes | nanoconfinement | photocatalytic interfaces | reactive oxygen species | sustainability | wastewater treatment | Z-scheme heterojunctions

ABSTRACT

Antibiotic-resistant bacteria (ARB) and antibiotic resistance genes (ARGs) persist in wastewater as chemically stable contaminants that evade conventional treatment, driving a global health crisis. Photocatalysis offers a promising route to simultaneously inactivate ARB and degrade ARGs. However, its practical implementation stays hindered by fundamental gaps in understanding how material interfaces control their fate. This review critically analyzes the interfacial battlefield, where surface chemistry, charge dynamics, and nanoconfinement determine the efficiency and mechanism of resistance destruction. We establish a quantitative reaction–diffusion framework that reveals why photocatalytic degradation is governed not by bulk-phase kinetics but by coupled transport–adsorption–reaction processes at the nanoscale interface. Through Damköhler analysis, we demonstrate that short-lived reactive oxygen species (ROS, $^{\bullet}OH$ diffusion < 10 nm) impose transport-limited regimes where adsorption and nanoconfinement become as critical as charge separation. We evaluate the dual target challenge: ARB as complex, multi-layered cellular structures requiring membrane disruption, and ARGs as persistent polyelectrolytes demanding complete mineralization. By examining how ROS with distinct lifetimes and diffusion distances operate at material interfaces, we establish that adsorption and nanoconfinement are as critical as charge separation. The review synthesizes recent advances in doping, heterojunction engineering (Z-scheme, S-scheme), defect creation, and carbon-based mediators through the cohesive perspective of interfacial design. Key gaps include unverified eARG mineralization, matrix scavenging, catalyst fouling and regeneration, biofilm and dormant cell formation after sublethal treatment, and insufficient life assessment. A roadmap is proposed toward selective, regenerable, matrix-tolerant and sustainability guided photocatalytic systems for antibiotic-resistance control.

1 | Introduction

Bacterial antimicrobial resistance (antibiotic resistance) constitutes a "silent pandemic" that claims > 750 000 deaths every year and is linked to 1.14 million deaths worldwide in 2021 [1–4]. Antimicrobial resistance is potentially leading to up to 10 million deaths annually by 2050 from infections involving resistant bacteria and threatens to decline global GDP by 3.80% by the same year [4–6]. Antibiotic resistance occurs when bacteria develop or acquire antibiotic resistance genes (ARGs) that significantly impair or negate the efficacy of standard antibiotic treatments against antibiotic resistant bacteria (ARB). Wastewater treatment plants (WWTPs) are recognized as critical hotspots for antibiotic resistance propagation, where horizontal gene transfer (HGT) among resistant bacteria facilitates the environmental dissemination of ARGs [7, 8].

Conventional disinfection, chlorination, ozonation, UV irradiation proves inadequate: it generates toxic by-products, induces reversible bacterial damage, and can paradoxically enrich resistant

populations through stress response [9–13]. Photocatalysis has emerged as a compelling alternative to control the spread of antibiotic resistance in WWTPs [14–18]. Light-induced generated reactive oxygen species (ROS) in the photocatalytic configurations cause disruption to the bacterial cell membrane, metabolic malfunction and oxidation of intracellular and extracellular DNA. Photocatalytic processes significantly reduce ARB/ARGs with complete inactivation of bacterial cells and considerable removal of ARGs [16, 17, 19, 20].

Over the last decade, research and development to improve visible-light photocatalytic activity and charge separation efficiency has transformed the photocatalysts from simple metal oxides (e.g., TiO_2, ZnO) to complex nanocomposites, heterojunctions and surface modified materials [21–24]. Coupled and hybrid systems such as solar-driven photo-Fenton process and sono-photocatalysis exhibit enhanced photocatalytic reactivity and improved removal efficiency [18, 25–27]. The application of emerging materials such as metal–organic frameworks (MOFs), carbon quantum dots (CQDs), and layered double hydroxides (LDHs) provide new opportunities to increase ROS production, extend the light absorption range, and minimize the charge recombination [17, 28–30]. Similarly, the recent advancements in engineered nanocomposites such as metal-modified graphitic carbon nitride and Fe-doped nanosheets have shown great potential to reduce the persistence of ARGs and inhibit genetic exchange [10, 15, 28, 29, 31].

Yet despite the intensive research encompassing TiO_2, ZnO, Bi-based oxyhalides, carbon nitrides, and innumerable composites, photocatalytic control of antibiotic resistance remains largely confined to laboratory scale. It signals a fundamental problem of aiming for a comprehensive list of materials over critical mechanistic understanding. Hence, some photocatalytic systems succeed while others fail against ARB/ARGs. The critical knowledge gaps that prevent moving from laboratory to practical applications precisely involve a lack of mechanistic understanding of photocatalytic configurations against ARB/ARGs, and a quantitative framework that explains interfacial constraints governing degradation efficiency. This review pinpoints this gap and reformulates the discourse to address the efficient photocatalytic inactivation of ARB/ARGs. We discuss that the photocatalytic interface, not the bulk material, constitutes the battlefield against ARB/ARGs. ARB and ARGs demand fundamentally different oxidative strategies, yet most studies treat them as equivalent endpoints. We analyze how cell wall complexity and DNA polyelectrolyte behavior dictate interfacial requirements. By examining ROS lifetimes and diffusion distances, we establish that short-lived species ($^{\bullet}OH$, $t_{1/2}$ ~10^{-9} s) require reactant adsorption at the catalyst surface, while longer-lived species (H_2O_2, $O_2^{\bullet-}$) can diffuse into bulk solutions. This perspective equates the importance of surface charge, nanoconfinement, and pore structure with that of bandgap engineering. Instead of discussing every composite that has been published, we extract mechanistic principles from successful studies, identify recurring issues, and propose a roadmap based on interfacial design, matrix tolerance, and sustainability metrics.

2 | The Dual Targets: ARB Versus ARGs

Effective photocatalytic design requires precise understanding of the targets. ARB and extracellular ARGs present chemically and structurally distinct challenges that demand tailored interfacial strategies. Table 1 summarizes the distinct characteristics and photocatalytic requirements for ARB versus ARGs.

2.1 | Antibiotic Resistant Bacteria: Multi-Layered Cellular Fortress

ARB possess complex cell envelopes that vary fundamentally between Gram-negative and Gram-positive lineages. Gram-negative bacteria (e.g., *Escherichia coli*, *Klebsiella pneumoniae*, *Pseudomonas aeruginosa*) feature an outer membrane rich in lipopolysaccharides (LPS), a thin peptidoglycan layer, and an inner cytoplasmic membrane [33, 35, 38]. This architecture functions as a sophisticated barrier: LPS confers negative surface charge (ζ-potential typically between −30 to −40 mV at neutral pH) while limiting penetration of hydrophobic and

TABLE 1 | Distinct characteristics and photocatalytic requirements for ARB versus ARGs [32–40].

Target	Structural features	Surface charge	Key vulnerability	Required photocatalytic strategy
ARB (Gram-negative)	LPS outer membrane, thin peptidoglycan	Negative (LPS, phospholipids)	Membrane integrity, electron transport chain	Membrane disruption, intracellular ROS penetration
ARB (Gram-positive)	Thick peptidoglycan, teichoic acids	Negative (teichoic acids)	Cell wall synthesis, membrane potential	Cell wall degradation, oxidative stress
iARGs (intracellular)	Protected by cytoplasm, proteins, membranes	—	DNA oxidation, replication inhibition	Sufficient ROS flux to overwhelm cellular defenses
eARGs (extracellular)	Phosphate backbone, base stacking	Strong negative	Phosphodiester cleavage, base modification	Adsorption, high-potential oxidation ($^{\bullet}OH$, h^+)

high-molecular-weight species [33, 35, 38]. Gram-positive bacteria (e.g., *Staphylococcus aureus*, *Enterococcus* spp.) lack the outer membrane but possess a thicker (20–80 nm) peptidoglycan layer that retains anionic teichoic acids, maintaining negative surface charge [33, 34, 36]. Intracellular ARGs reside within these protective environments in ARB, shielded by multiple membranes and cytoplasmic components that scavenge ROS before they reach DNA targets [32].

Complete ARB inactivation and iARG damage therefore require more than contact between cells and photocatalyst particles. A credible mechanism should include: (i) membrane or cell-wall disruption that compromises barrier function, (ii) penetration or intracellular generation of oxidative species, (iii) damage to multiple biomolecular targets including proteins, lipids, and nucleic acids, and (iv) post-treatment evidence that injured cells do not repair or regrow. In this context, iARG mineralization is not treated as a direct primary endpoint because iARGs are shielded by membranes, cytoplasm, and scavenging biomolecules; they become accessible for direct mineralization mainly after cell lysis or release as eARGs [32, 41].

2.2 | Antibiotic Resistance Genes: Persistent Polyelectrolytes

Extracellular ARGs (eARGs) liberated from lysed cells present an orthogonal challenge. DNA is a polyanionic polymer (phosphate backbone pKa ≈ 2) with remarkable chemical stability [40]. The phosphodiester bonds require high oxidation potential ($E° > 1.9$ V) for cleavage, while purine and pyrimidine bases demand different ROS for effective modification [37]. Effective eARG degradation therefore requires electrostatic capture, base/backbone oxidation and verification that residual fragments no longer retain biological functions. eARGs have a linear charge density of approximately -2e per 0.34 nm (one negative charge per phosphate), so they are strongly attracted to the positively charged surfaces. Because the Debye length (κ^{-1}) in typical wastewater (ionic strength ≈ 10–50 mM) is only about 1–3 nm, this electrostatic enrichment occurs only in the immediate vicinity of charged interfaces [39, 42, 43].

Guanine has the lowest ionization potential among nucleobases, making guanine-cytosine (GC)-rich genes more susceptible to one-electron oxidation. Genes with high GC content, such as sulfonamide resistance genes (e.g., *sul*1, and *sul*2), are consequently more vulnerable to photogenerated hole attack than AT-rich genes (e.g., *tet*A) [44, 45]. However, qPCR signal loss alone is insufficient evidence of mineralization because partially degraded fragments can retain transformation potential or be repaired by competent bacteria [46, 47]. Table 2 presents the operational endpoints and levels of evidence for managing ARB and ARGs.

3 | Reactive Oxygen Species as Spatially Constrained Weapons

Photocatalysis generates a suite of ROS with distinct oxidation potentials, lifetimes, and diffusion distances. These differences

TABLE 2 | Operational endpoints and evidence levels for photocatalytic control of ARB and ARGs.

Endpoints	Common measurements	Inference	Limitations	Additional measurements (stronger evidence)	References
ARB inactivation	CFU reduction, live/dead staining, ATP or respiratory activity assays	Loss of culturability, membrane/metabolic damage	CFU loss may miss VBNC or dormant cells	Regrowth tests, viability assays	[48, 49]
iARG damage	Intracellular qPCR/PMA-qPCR after cell separation	Reduced detectable gene copies inside cells	Unclear mineralization	Irreversible cell death and loss of gene transfer potential	[48, 50, 51]
eARG degradation	qPCR/dPCR amplicon loss, gel electrophoresis, fragment size analysis	Short region DNA damage or fragmentation	Short amplicons cannot distinguish complete gene destruction from partial fragmentation	Fragment size profiling, functional assays	[14, 46, 47, 50, 51]
Mineralization	TOC/DOC removal, LC–MS/HRMS degradation products, inorganic N and P release	Conversion beyond fragments toward small molecules, CO_2, NH_3/NOx, phosphate	Energy intensive, rarely demonstrated for trace eARGs in real matrices	Mineralization differentiation from qPCR loss/fragmentation	[48, 49, 52, 53]

Abbreviations: CFU, colony forming units; dPCR, digital PCR; LC-MS/HRMS, liquid chromatography-mass spectrometry/high-resolution mass spectrometry; PMA-qPCR, propidium monoazide-qPCR; TOC/DOC, total/dissolved organic carbon; VBNC, viable nut non-culturable.

TABLE 3 | Physiochemical properties of major ROS relevant to ARB/ARGs inactivation [15, 54, 55].

ROS	Oxidation potential (E^0, V)	Lifetime (Half-life, $t_{1/2}$)	Migration distance	Primary targets
Hydroxyl radical ($^{\bullet}OH$)	2.80	10^{-9} s	< 10 nm	Lipids, proteins, DNA bases/backbone
Sulfate radical ($SO_4^{\bullet-}$)	2.5–3.1	$3–4\times10^{-5}$ s	~30 nm	Aromatic rings, unsaturated bonds
Singlet oxygen ($^1O_2$)	2.25	10^{-6}–10^{-3} s	~100 nm	Guanine, unsaturated lipids.
Hydrogen peroxide (H_2O_2)	1.78	minutes to hours	mm–cm	Fenton chemistry, signaling
Superoxide ($O_2^{\bullet-}$)	0.94	10^{-6} s	~100 nm	Fe-S clusters, lipid peroxidation

determine whether oxidative damage occurs mainly at the photocatalyst surface, within the hydrodynamic boundary layer, or inside bacterial cells. Table 3 quantifies these differences, which are critical for rational interface design.

In a photocatalytic configuration, upon photoexcitation, valence band holes (h^+) and conduction band electrons (e^-) migrate to the surface, where they participate in redox reactions with adsorbed H_2O, OH^- and O_2 [20, 41, 56, 57].

$$H_2O + h^+ \rightarrow {}^{\bullet}OH + H^+ \quad (1)$$

$$OH^- + h^+ \rightarrow {}^{\bullet}OH \quad (2)$$

$$O_2 + e^- \rightarrow O_2^{\bullet-} \quad (3)$$

$$O_2^{\bullet-} + H^+ \rightarrow HO_2^{\bullet} \quad (4)$$

$$2HO_2^{\bullet} \rightarrow H_2O_2 + O_2 \quad (5)$$

$$O_2^{\bullet-} + h^+ \rightarrow {}^1O_2 \quad (6)$$

$$H_2O_2 + e^- \rightarrow OH^- + {}^{\bullet}OH \quad (7)$$

The extremely short lifetime and < 10 nm diffusion distance of $^{\bullet}OH$ mean that $^{\bullet}OH$ mediated oxidation requires adsorbed or nonconfined targets. This does not imply that $^{\bullet}OH$ is the only biologically relevant ROS. Longer lived species such as H_2O_2 and $O_2^{\bullet-}$ contribute through different routes: H_2O_2 can diffuse across or through bacterial envelopes and participate in intracellular Fenton-type reactions that generate secondary $^{\bullet}OH$, whereas $O_2^{\bullet-}$ can damage Fe-S clusters, disturb redox metabolism and amplify oxidative stress [41, 54, 58]. Thus, surface-bound $^{\bullet}OH$ is central to eARG oxidation, while intracellular oxidative injury in ARB is often produced by a coupled cascade involving H_2O_2, $O_2^{\bullet-}$, holes and secondary $^{\bullet}OH$.

Optimal ARB inactivation therefore requires interfaces that promote attachment without excessive fouling, concentrate cells near ROS-generation sites and sustain ROS flux long enough to exceed cellular repair capacity. In contrast, eARG degradation relies more strongly on surface-mediated oxidation because the negatively charged phosphate backbone can adsorb to positively charged domains, positioning DNA within the short reaction radius of $^{\bullet}OH$ or direct hole transfer. This mechanistic interpretation is synthesized from prior photocatalytic and oxidative-stress studies rather than proposed as a universal conclusion from a single experiment [39, 41, 54, 58–61]. After identifying the unique needs of ARB and ARGs and considering the spatial limitations of ROS, we now explore how the design of materials influences the interfacial microenvironment.

4 | Reaction–Diffusion Constraints

Photocatalytic inactivation of ARB and degradation of ARGs are frequently described using apparent pseudo-first-order kinetics. Although this treatment is convenient for comparing experimental datasets, it conceals the fact that heterogeneous photocatalysis is fundamentally an interfacial process in which adsorption, charge transfer, radical generation, and oxidation occur predominantly at or near the catalyst surface. Classic photocatalysis literature has long emphasized that overall reaction rates are jointly governed by photon absorption, charge-carrier dynamics, surface reaction kinetics, and transport of reactants to active sites rather than by bulk concentration decay alone [62–64].

Accordingly, many studies report target removal using an apparent pseudo-first-order model:

$$\frac{dC_b}{dt} = -k_{app}C_b \quad (8)$$

where C_b is the bulk concentration (ML^{-3}) of the target species and k_{app} is an apparent pseudo-first-order rate constant (T^{-1}). Although this formulation provides a convenient way to compare catalytic performance, it implicitly assumes homogeneous ROS distribution, instantaneous mixing, and negligible transport limitations. These assumptions are rarely valid in photocatalytic systems because many ROS, particularly hydroxyl radicals ($^{\bullet}OH$), have extremely short lifetimes ($\leq 10^{-9}$ s) and diffusion lengths of only a few nanometers. As a result, oxidation reactions occur almost exclusively at or extremely close to the catalyst surface. This spatial limitation implies that photocatalytic destruction of ARB and ARGs is fundamentally governed by reaction–diffusion coupling at the photocatalytic interface rather than by bulk-phase kinetics [65–67].

4.1 | Interfacial Reaction–Diffusion Framework

A more physically meaningful description separates diffusion through the liquid boundary layer from reaction at the photocatalyst surface. The concentration profile of a target species near the photocatalyst surface can be described using the classical reaction–diffusion equation.

$$\frac{\partial C}{\partial t} = D_{eff}\frac{\partial^2 C}{\partial x^2} - R(C) \tag{9}$$

where $C(x,t)$ represents the concentration (ML^{-3}) of the target compound (e.g., extracellular DNA fragments or cell-associated biomolecules), D_{eff} is the effective diffusion coefficient (L^2T^{-1}) of the target compound in the hydrodynamic boundary-layer thickness, and R denotes the interfacial reaction rate (T^{-1}).

Under steady-state conditions the governing equation reduces to:

$$D_{eff}\frac{\partial^2 C}{\partial x^2} = R(C) \tag{10}$$

with boundary conditions defined by the catalyst surface and the bulk solution. At the interface ($x=0$), the diffusive flux of the target species equals the net interfacial reaction rate, while at the outer boundary layer the concentration approaches the bulk concentration (C_b).

Solutions to this equation reveal a concentration gradient within the hydrodynamic boundary layer, indicating depletion of reactants near the photocatalyst surface when reaction rates exceed transport rates. Such gradients are commonly observed in heterogeneous catalysis and environmental reaction systems where interfacial processes dominate overall kinetics [67, 68].

4.2 | Adsorption-Controlled Photocatalytic Reactions

Because ROS operate only within nanometer-scale distances from the catalyst surface, effective degradation requires adsorption or close proximity of targets to the catalytic interface. This behavior is often described using Langmuir-type adsorption kinetics: [62, 68, 69]

$$\theta = \frac{(K_{ads}C_s)}{(1 + K_{ads}C_s)} \tag{11}$$

where θ represents the fractional surface coverage, C_s is the concentration adjacent to the surface (ML^{-3}), and K_{ads} is the adsorption equilibrium constant (L^3M^{-1}). The corresponding Langmuir-Hinshelwood-type surface reaction rate can then be expressed as follows:

$$r = k_{react}\theta \tag{12}$$

where k_{react} is the first-order oxidation frequency of the adsorbed target. Combining these relations yields a Langmuir–Hinshelwood-type expression widely applied in photocatalysis:

$$r = \frac{(k_{react}K_{ads}C_s)}{(1 + K_{ads}C_s)} \tag{13}$$

This formulation demonstrates that degradation rates are strongly influenced by adsorption affinity. For extracellular ARGs, the negatively charged phosphate backbone promotes electrostatic attraction to positively charged photocatalyst surfaces, increasing surface coverage and enhancing reaction probability. In contrast, bacterial cells must first attach to the photocatalyst surface before oxidative attack can occur. Consequently, interfacial adsorption and attachment processes play a critical role in determining overall photocatalytic efficiency [63, 69, 70].

4.3 | Reaction-Transport Coupling and Damköhler Analysis

The relative importance of interfacial reaction and mass transfer can be quantified using the Damköhler number (D_a):

$$D_a = \frac{(k_s L)}{D_{eff}} = \frac{k_s}{k_m} \tag{14}$$

where k_s is the surface reaction rate constant (T^{-1}), k_m is the mass-transfer coefficient (T^{-1}), and L represents the characteristic diffusion length (L) (e.g., boundary-layer thickness) [65–67].

Two limiting regimes can be distinguished. When $D_a << 1$, overall removal is reaction-limited and improvements in intrinsic catalytic activity are most beneficial. When $D_a >> 1$, the system becomes transport-limited, meaning that even if the catalyst generates ROS efficiently, the observed rate is constrained by delivery of the target to the interface. Analyses of photocatalytic reactors have shown that mass-transfer limitations are not negligible under many operating conditions, particularly where boundary layers are thick, catalyst agglomeration occurs, or pore accessibility is restricted [67].

For photocatalytic reactions involving short-lived radicals such as $^{\bullet}OH$, the effective Damköhler number is typically large, indicating transport-limited behavior. In this regime, improvements in photocatalyst performance require strategies that increase the probability of target molecules entering the ROS reaction zone rather than simply increasing ROS generation [64–67]. However, the actual regime depends on catalyst loading, mixing intensity, particle aggregation, pore accessibility, light distribution, matrix scavenging, and the size and diffusivity of the target. This point is especially important for ARB because bacterial transport and attachment are not governed by molecular diffusion alone.

4.4 | Interfacial Residence Time and Probability of Oxidative Degradation

Nanoconfinement improves photocatalytic performance not merely by increasing adsorption, but by increasing the time that targets remain within the reactive interfacial zone. Interfacial residence time strongly influences photocatalytic degradation efficiency because heterogeneous photocatalytic reactions occur mainly at or near the catalyst surface, where adsorption, desorption, radical generation, and interfacial oxidation are coupled [62–64, 67–70]. Adsorbed targets remain

exposed to ROS flux for mean residence time determined by desorption kinetics:

$$\tau_{res} = \frac{1}{k_{des}} \quad (15)$$

where k_{des} is the apparent first-order desorption rate constant (T^{-1}). The probability (p) that an adsorbed molecule undergoes oxidative degradation during this residence period can be approximated as follows:

$$p = 1 - e^{(-k_{react}\tau_{res})} \quad (16)$$

This expression reflects a first-order interfacial reaction probability during the mean residence time and indicates that degradation becomes more likely when adsorption is sufficiently long-lived relative to the oxidation frequency [65, 66, 68, 69]. Materials that increase adsorption strength or create nanoconfined environments can therefore enhance degradation efficiency by increasing residence time (τ_{res}) and cumulative ROS exposure. Hierarchical porous structures, layered materials, and graphene-based architectures have been shown to promote such nanoconfinement effects, effectively trapping bacteria or DNA fragments within the diffusion range of reactive radicals [39, 46, 61, 71]. For ARB, the same principle applies at a larger scale: attachment and confinement increase local exposure to surface-bound ROS, but irreversible inactivation also requires sufficient oxidative damage to membranes, proteins, and intracellular components to prevent repair and regrowth.

4.5 | Mechanistic Implications for Photocatalyst Design

The reaction–diffusion framework provides a mechanistic explanation for experimental trends in photocatalytic ARB/ARG studies (Figure 1). First, surface charge engineering enhances electrostatic attraction between photocatalysts and negatively charged bacterial membranes or DNA molecules, increasing adsorption (K_{ads}) and effective reaction rates [33, 39, 46, 61, 72–77]. Second, hierarchical or porous structures promote nanoconfinement, ensuring that targets remain within the limited diffusion radius of short-lived ROS [14, 39, 61, 71]. Third, defect engineering and heterojunction design increase ROS generation rates (k_{react}), improve charge separation, and extend charge-carrier lifetimes, thereby raising oxidant flux at the interface [14, 15, 61, 78–90]. Finally, conductive carbon mediators improve electron transport and sustain ROS production, maintaining oxidative capacity during interfacial reactions [21–23, 55, 71, 91–94].

Taken together, these mechanisms indicate that photocatalytic performance is governed not only by intrinsic material properties such as bandgap and light absorption but also by the ability of photocatalysts to regulate transport, adsorption, and reaction processes at the nanoscale interface [62–64, 67, 68]. This perspective highlights the photocatalytic interface as the central arena where ARB and ARG destruction occurs and provides the mechanistic foundation for the material-engineering strategies discussed in the following section.

5 | Engineering the Photocatalytic Interface: Mechanistic Principles

To advance material designs for controlling the interfacial microenvironment, we extracted mechanistic principles from four strategic domains: surface charge engineering, charge carrier direction, defect-mediated activation, and conductive mediation.

5.1 | Surface Charge and Nanoconfinement

The electrostatic attraction between photocatalyst surfaces and negatively charged ARB/ARGs constitutes the first and most critical step in the degradation cascade [72, 74]. Zeta (ζ) potential measurements reveal that most bacterial cells maintain negative surface charges at pH higher than 2 due to the predominance of negatively charged functional groups associated with peptidoglycan, teichoic acid, and teichuronic acid on the surface of gram-positive bacteria and with lipopolysaccharide (LPS), phospholipids, and proteins on the surface of gram-negative bacteria [33, 76, 77], while DNA exhibits strong negative charge density from phosphate backbone ionization [73, 75].

Bismuth oxyhalides (BiOX) demonstrate the power of surface charge engineering [95–97]. The layered BiOCl structure consists of positively charged $[Bi_2O_2]^{2+}$ slabs alternately stacked with Cl^- layers, generating an intrinsic internal electric field along the c-axis and perpendicular to the (001) facets [96]. As shown by electron difference density maps and Mulliken charge analysis (Figure 2a–c), interfacial charge redistribution produces distinct positive and negative domains, confirming self-induced polarization. When facet orientation is tuned (e.g., BiOI(001)/BiOCl(010)), the internal field reorients parallel to the heterojunction plane, shortening electron diffusion distance and enhancing charge-injection efficiency, as schematically illustrated in Figure 2d. This nanoconfined, directional carrier transport suppresses recombination, while the positively polarized $[Bi_2O_2]^{2+}$ layers provide electrostatically favorable adsorption sites for anionic species, coupling surface charge engineering with improved interfacial reaction kinetics.

Yu et al. [61] demonstrated this principle through a Z-scheme Bi/BiOCl/Bi(In^{3+})-MOF heterojunction. The composite exhibited strongly positive ζ-potential (+25 to +35 mV across pH 4–9), resulting in rapid electrostatic capture of both *E. coli* ARB and *tet*A ARG fragments. This local preconcentration effect, described as nanoconfinement, shortened diffusion distances between targets and surface-bound •OH and enabled 4.89-log removal of *tet*A genes within 2 h. However, this advantage should be interpreted as an initial interfacial enrichment effect rather than an indefinitely sustainable property; repeated operation requires regeneration to remove cell debris, adsorbed DNA, and matrix foulants that would otherwise mask active sites.

Hierarchical architecture amplifies nanoconfinement and interfacial charge regulation. Li et al. [71] engineered NRGO-wrapped $Bi_2O_2CO_3$ microspheres, where the core–shell structure (Figure 3a–f) creates a nanoconfined interface that localizes bacteria near reactive sites, while nitrogen doping tunes surface electrostatics to enhance adsorption affinity (Figure 3e). This

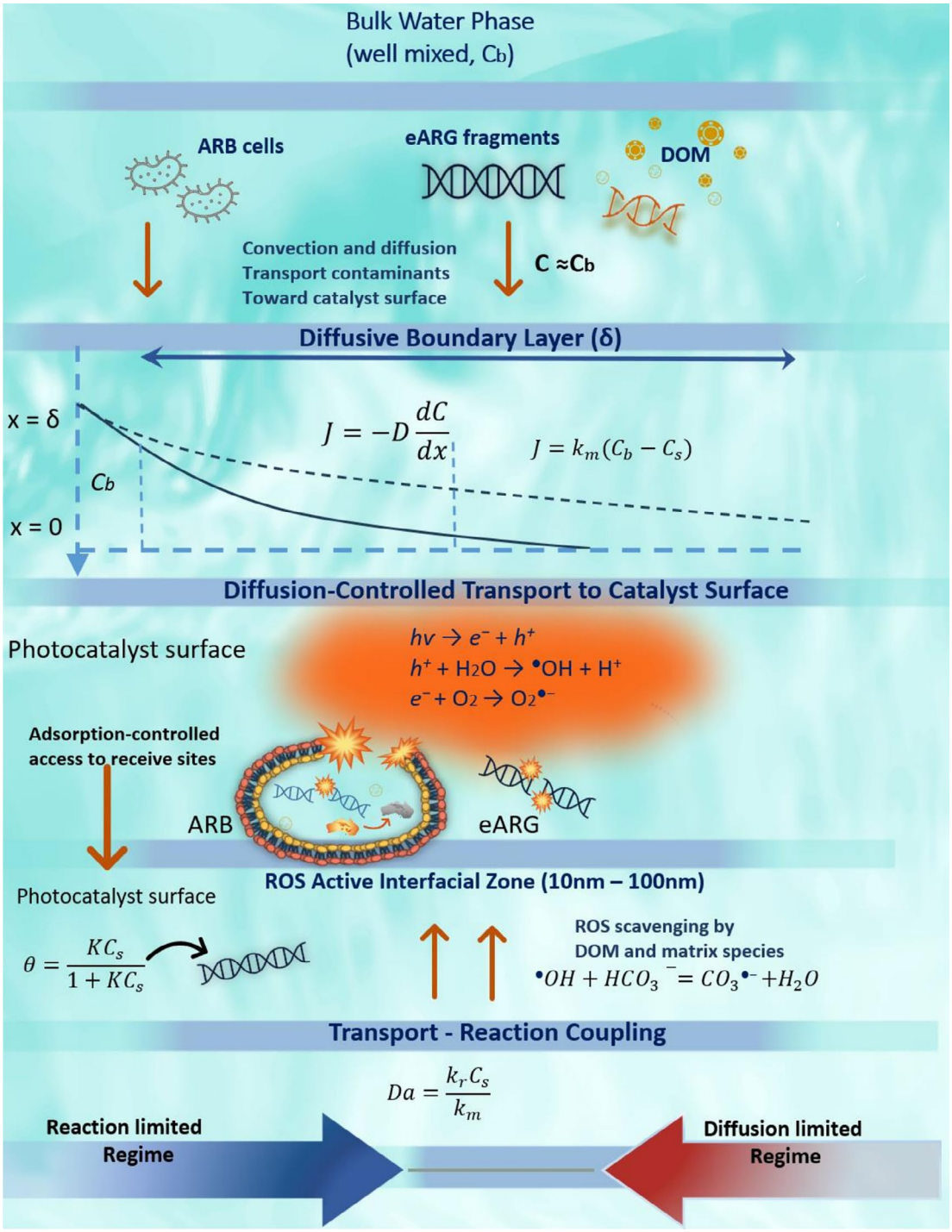

FIGURE 1 | The reaction–diffusion framework for photocatalytic inactivation of ARB and ARGs.

interfacial coupling accelerates charge transfer (carrier lifetime reduced from 55.3 to 19.8 ns), extends light absorption to 459 nm, and promotes ~3-fold higher ROS generation while improving photocatalyst stability. The NRGO shell additionally suppresses photocorrosion, improving catalytic stability and operational lifespan.

Accordingly, effective photocatalyst design should move beyond maximizing positive surface charge or adsorption capacity alone. Materials must balance target capture, ROS generation, pore accessibility, and cleanability so that ARB/ARGs are retained within the •OH reaction radius without promoting irreversible fouling, residual biomass accumulation, or secondary biofilm formation during repeated use.

5.2 | Charge Carrier Direction

The recombination of photogenerated electrons and holes remains the primary efficiency bottleneck in photocatalysis [80, 86, 90].

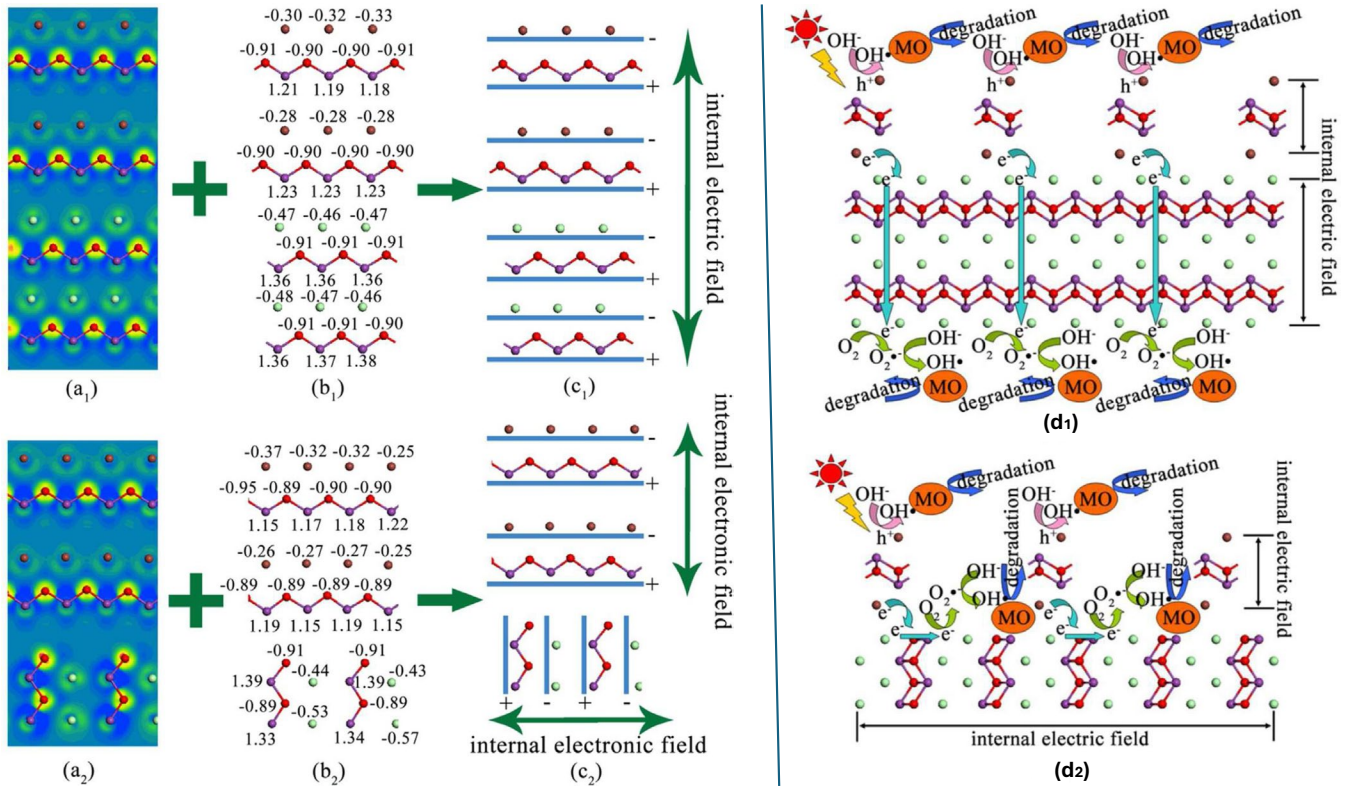

FIGURE 2 | Surface charge engineering and facet-dependent photocatalytic mechanism at BiOI/BiOCl heterointerfaces. Electron density redistribution and charge population analysis (a–c) reveal self-induced internal electric fields arising from layered polarization, directing carrier migration. The resulting facet-dependent pathways (d) enhance charge separation, reactive oxygen species generation, and pollutant degradation through nanoconfined charge transport. Reprinted with permission from [96]. Copyright 2015, American Chemical Society.

Type-II heterojunctions have been widely used to address this issue by facilitating charge separation. However, they often suffer from reduced redox potential, as electrons and holes migrate to lower conduction bands (CB) and higher valence bands (VB), respectively, which diminishes their oxidation and reduction capabilities [83]. Z-scheme and S-scheme heterojunctions overcome this limitation by preserving high-energy charge carriers [84, 85]. In a direct Z-scheme, the CB electron from one semiconductor recombines with the VB hole from another, leaving the high-potential CB electron of the second and the high-potential VB hole of the first available for redox reactions [89]. Yu et al. [61] demonstrated two charge-transfer pathways for the Bi/BiOCl/Bi(In^{3+})-MOF system (Figure 4). In the Type-II heterojunction model, electrons migrate to Bi^0 (Ef = −0.17 eV), which is thermodynamically insufficient to reduce O_2 to $O_2^{\bullet-}$ (−0.33 eV). The Z-scheme pathway, mediated by Bi^0 as an electron bridge and an internal electric field, retains electrons on the BiOCl CB (−0.75 eV) and holes on the MOF VB (2.99 eV). This directional recombination preserves strong redox potentials, enabling simultaneous $O_2^{\bullet-}$ and $^{\bullet}OH$ formation that oxidatively damages cell membranes and intracellular biomolecules.

S-scheme (step-scheme) heterojunctions represent an evolution beyond conventional Type-II systems, specifically designed to preserve strong redox potentials in particulate photocatalysts. The $NiFe_2O_4/Bi_2WO_6$/ZnO photocatalyst developed by Lam et al. [81] operates via an S-scheme charge-transfer mechanism, where ZnO nanorods (CB ≈ −0.42 V, VB ≈ +2.68 V) and Bi_2WO_6 (CB ≈ +0.40 V, VB ≈ +3.18 V) establish an internal electric field after Fermi-level equilibration (Figure 5). Under illumination, photogenerated electrons in Bi_2WO_6 recombine selectively with holes from ZnO at the interface, eliminating low-energy carriers while retaining highly reducing electrons on ZnO and strongly oxidizing holes on Bi_2WO_6. This directional carrier filtering enhances charge separation without sacrificing redox capability, thereby promoting efficient reactive oxygen species generation and improved photocatalytic performance. Overall, Z-scheme and S-scheme architectures are superior for photocatalytic $^{\bullet}OH$ generation because they maintain high-potential charges, whereas Type-II causes high-energy electrons/holes to migrate to lower-energy bands, significantly reducing redox potential. S-schemes, in particular, use internal electric fields to recombine low-energy carriers, preserving strong oxidative holes in the valence band for $^{\bullet}OH$ production.

5.3 | Defect Engineering

Oxygen vacancies (OVs) and other point defects modulate electronic structure, light absorption, and surface reactivity of metal oxides through multiple mechanisms. These defects influence the material properties through mechanisms such as bandgap narrowing, charge trapping, and adsorption activation [87]. OVs introduce mid-gap states 0.5–1.5 eV below the conduction band, which extend light absorption into visible and near-infrared regions. OVs localize photogenerated electrons to suppress

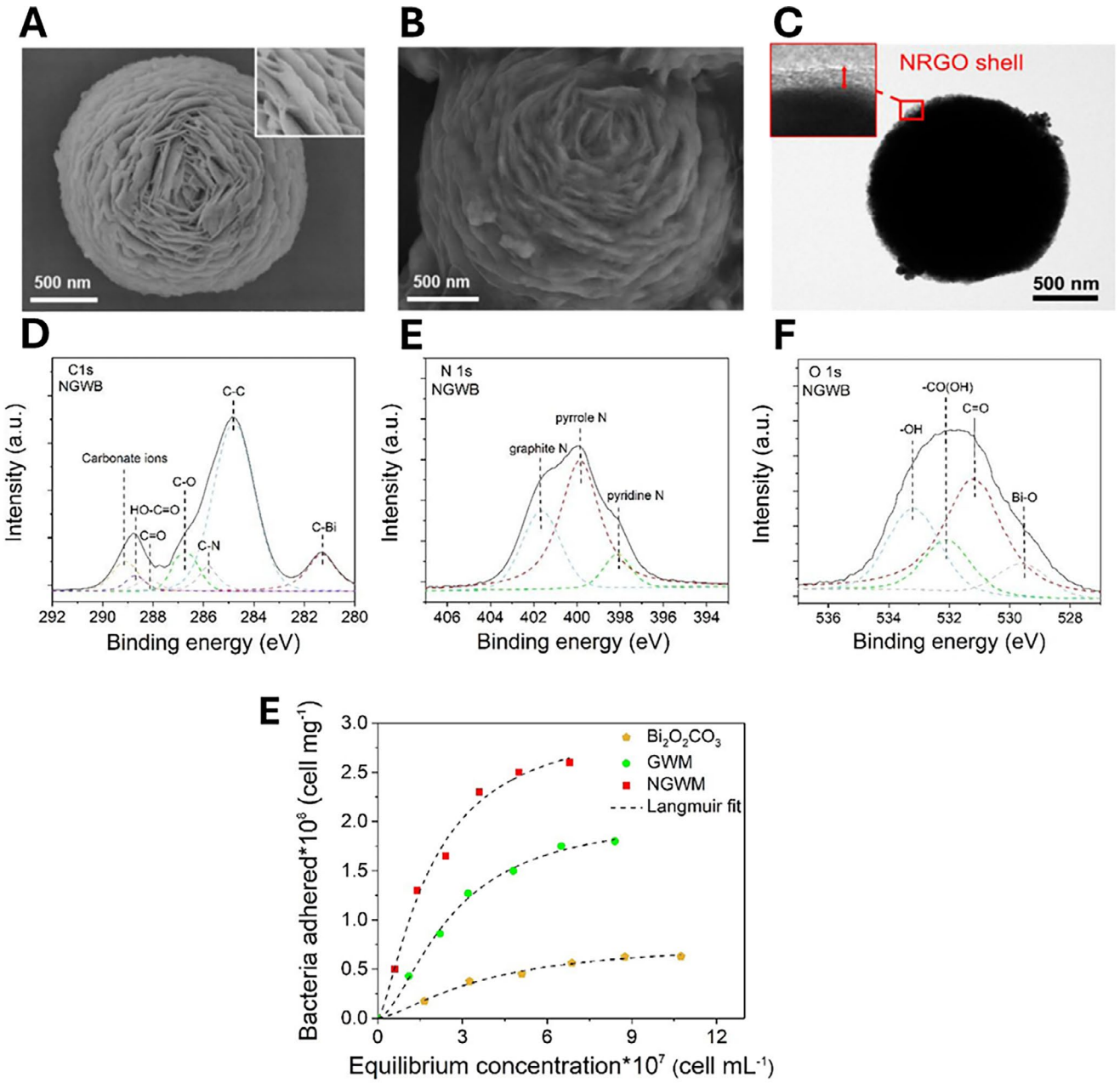

FIGURE 3 | Structural and interfacial characterization of NRGO-wrapped $Bi_2O_2CO_3$ hierarchical photocatalyst. (A) SEM image showing hierarchical $Bi_2O_2CO_3$ microspheres assembled from nanosheets. (B) SEM image of the NRGO core–shell structure. (C) HR-TEM image confirming a thin NRGO shell (~10–15 nm) forming a nanoconfined interface. (D–F) XPS spectra revealing interfacial C–Bi bonding and nitrogen doping (pyridinic, pyrrolic, and graphitic N), evidencing strong electronic coupling between the $Bi_2O_2CO_3$ core and NRGO shell that facilitates interfacial charge transfer. (E) Enhanced bacterial adsorption resulting from nitrogen-induced surface charge modulation, enabling surface-bound ROS oxidation pathways. Reprinted with permission from [71]. Copyright 2020, Elsevier.

recombination, increase carrier lifetime and binding energy for O_2 and H_2O, and promote ROS generation for inactivation of ARB/ARGs in aquatic systems [78, 79, 82, 88].

Wang et al. [87] engineered oxygen vacancy-mediated Bi_2WO_6/FeOOH heterojunctions (Vo-BWO/FeOOH) for photo-Fenton ARB inactivation. The Vo-rich sample (Vo-r-BWO/FeOOH) exhibited: (i) accelerated interfacial charge migration; (ii) enhanced H_2O_2 adsorption and activation; (iii) 94.1% inactivation of tetracycline-, ampicillin-, and kanamycin-resistant *E. coli* within 80 min; and (iv) complete tetracycline degradation (100%) within 60 min. The oxygen vacancies functioned as electron traps, facilitating Fe^{3+}/Fe^{2+} cycling and sustaining $^{\bullet}OH$ production through Fenton chemistry. This exemplifies defect-mediated synergy between photocatalysis and classical Fenton processes.

Gao et al. [15] demonstrated that carbon vacancies in g-C_3N_4 create localized electronic traps that function as reactive hotspots (Figure 6). Deformation charge density mapping reveals electron accumulation at C–$(N)_3$ defect sites, promoting charge separation and directing electrons toward surface reactions. These

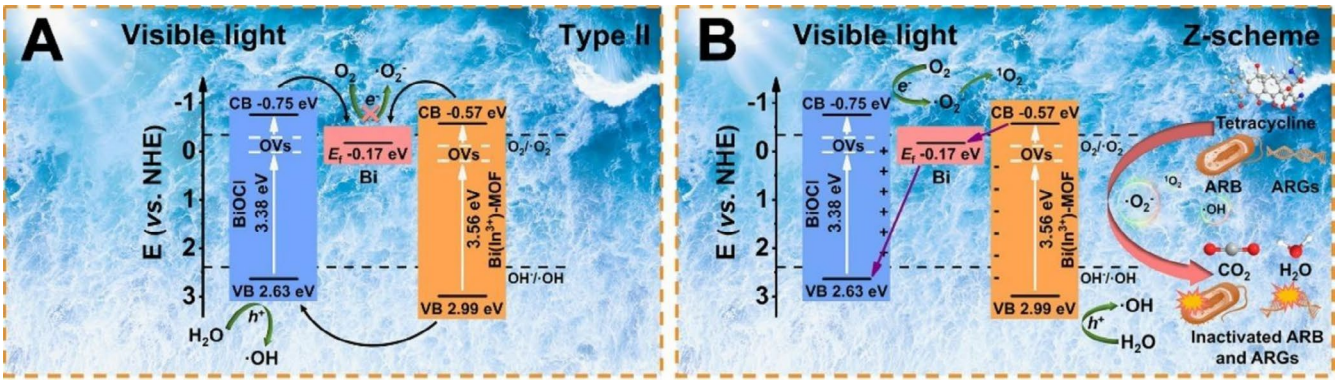

FIGURE 4 | Two possible photodegradation mechanisms: (A) type II heterojunction—passive charge separation and (B) Z-scheme heterojunction—directed charge flow. Reproduced with permission from [61]. Copyright 2025 Elsevier.

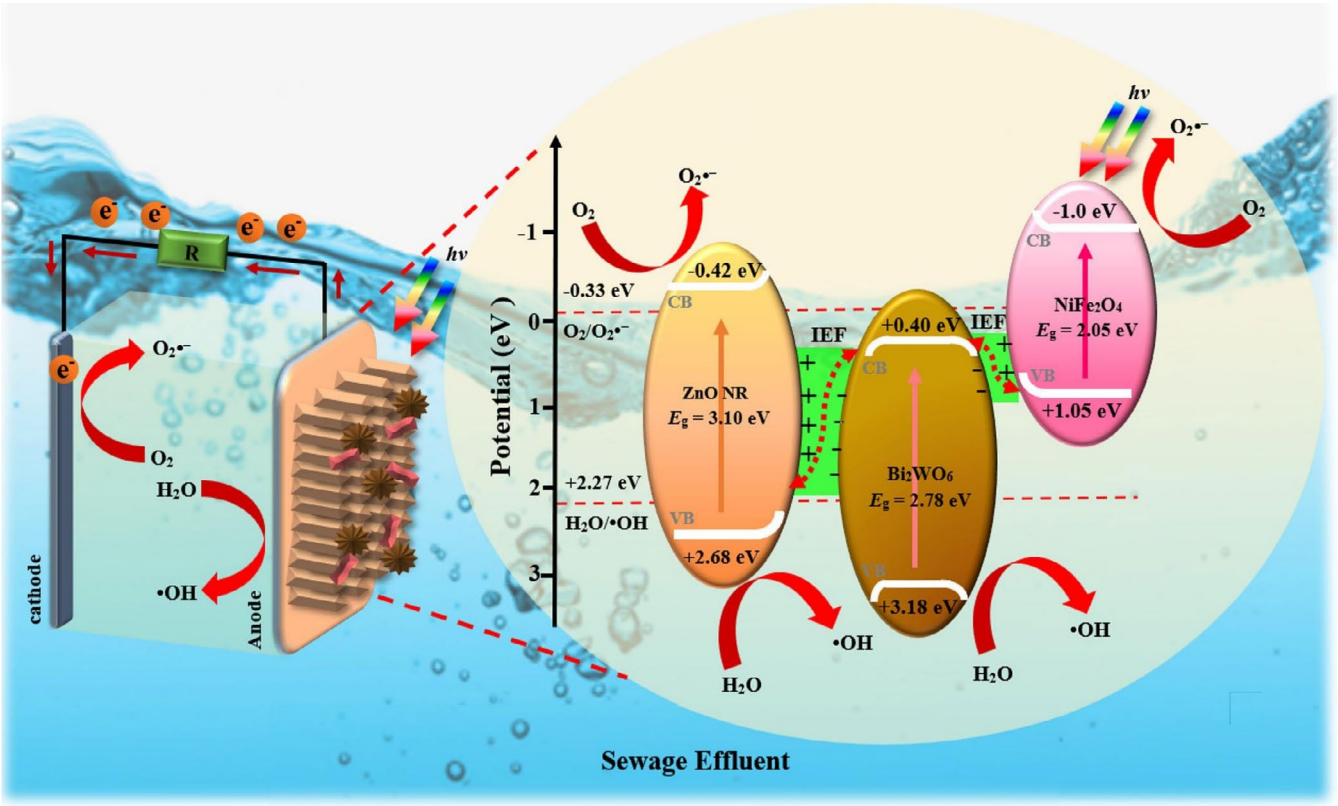

FIGURE 5 | Dual S-scheme $NiFe_2O_4/Bi_2WO_6/ZnO$ nanorod array photoanode showing internal electric-field-mediated charge transfer and enhanced photocatalytic activity in a photocatalytic fuel cell. Reprinted with permission from [81]. Copyright 2025, Elsevier.

vacancy centers strengthen persulfate adsorption and elongate the O–O bond (1.505 → 1.519 Å), enabling efficient $SO_4^{\bullet-}$ generation. Consequently, defect-engineered CN-C_{V2}/PS exhibits rapid ROS production, achieving 6.5-log ARB inactivation and 4.8–6.7-log eARGs removal.

Defect engineering regulates the electronic structure and surface reactivity, creating electron-rich hotspots that promote charge separation and catalytic activation. However, sustained photocatalytic efficiency also requires rapid charge transport beyond localized defect sites. In this context, conductive carbon materials function as electron highways, enabling efficient interfacial electron migration and improving charge utilization for continuous ROS generation.

5.4 | Conductive Mediators

Carbon-based materials—graphene, reduced graphene oxide (rGO), carbon nanotubes (CNTs), carbon quantum dots (CQDs)—function not as primary photocatalysts but as conductive electron mediators that extract and shuttle photogenerated charges. Their high carrier mobility (up to ~2×10^5 cm^2/V.s for high quality graphene) enables rapid electron transfer from

semiconductor conduction band to surface redox sites, thereby suppressing recombination and accelerating interfacial reactions [55, 91, 94].

Graphene acts as a conductive mediator forming electron-transport highways. Ilkhas et al. [92] developed a ternary Cu-doped ZnO/rGO nanocomposite that exemplifies the synergistic roles of defect engineering and conductive mediation. TEM/SEM images (Figure 7a,b) reveal ZnO nanoparticles uniformly anchored on graphene sheets, creating a continuous conductive network that efficiently extracts photogenerated electrons. Consistently, the markedly reduced photoluminescence intensity of Cu-ZnO/GP (Figure 7c) indicates suppressed electron–hole recombination arising from rapid electron migration into graphene. This carbon-mediated charge delocalization prolongs carrier lifetime and enhances interfacial redox reactions, demonstrating that carbon materials function as electron highways rather than primary photocatalysts.

CQDs offer additional quantum confinement effects. Jin et al. [93] consolidated CQDs with NiFe-MOF in photo-Fenton membranes, achieving 84.9% rifampicin degradation and potent antibacterial activity against both Gram-positive and Gram-negative pathogens. The CQDs served dual functions, up-converting near-IR light to visible and facilitating electron transfer to Fe centers (electron transfer efficiency increased 2.3-fold). Integrating conductive carbon architectures as electron mediators can significantly enhance photocatalytic processes by extending carrier lifetimes, suppressing recombination, and enabling multi-electron reduction pathways such as $O_2 \rightarrow H_2O_2 \rightarrow {}^{\bullet}OH$. This approach leverages the unique properties of carbon materials to improve charge separation and transfer, which are critical for efficient photocatalysis.

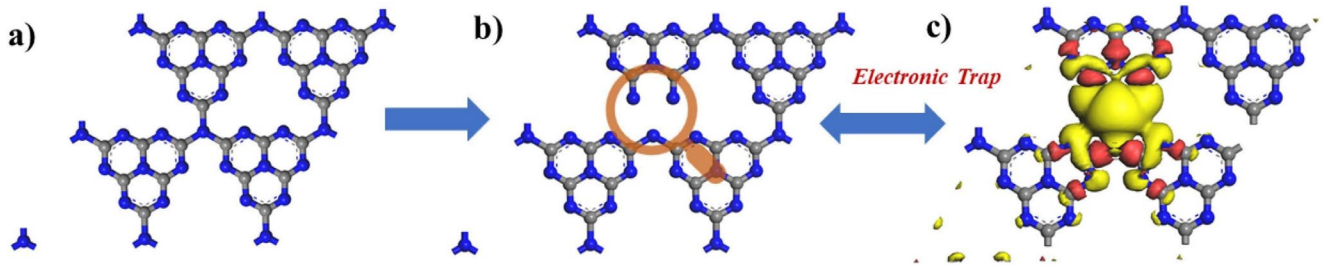

FIGURE 6 | The structure of CN (a) and CN-C (b, c) the electronic trap of CN-CV2 (The yellow and red cloud densities represent the electron enrichment and electron depletion, respectively). Reprinted with permission from [15]. Copyright 2021, Elsevier.

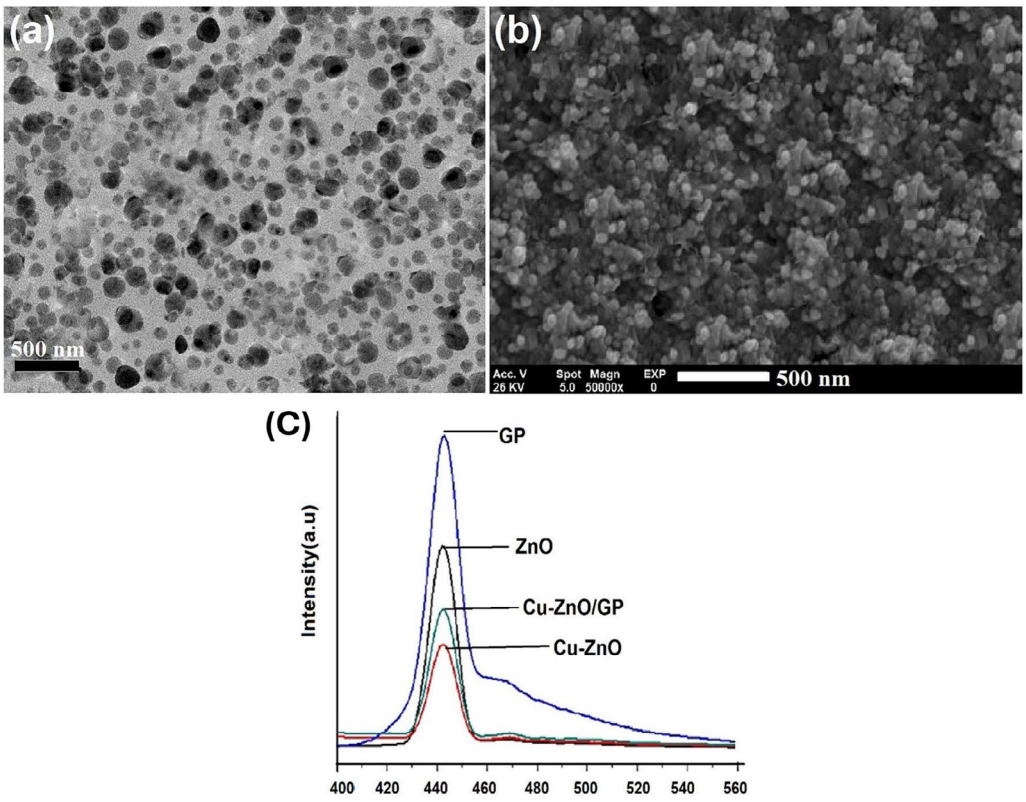

FIGURE 7 | The TEM (a) and FE-SEM (b) images of Cu-ZnO/GP catalyst and photoluminescence (PL) spectra (c) of ZnO, Cu-ZnO, GP, and Cu-ZnO/GP. Reprinted with permission from [92]. Copyright 2024, Elsevier.

6 | Critical Knowledge Gaps and Challenges

Despite significant advances, critical obstacles hinder the practical application of photocatalytic ARB/ARGs control. We highlight three major challenges and suggest corresponding research pathways.

6.1 | eARGs Mineralization

Conventional evaluation of ARGs removal is predominantly based on qPCR quantification, which measures short amplicons (approximately 100–200 bp) and therefore cannot distinguish between intact functional genes and partially degraded fragments [50, 51]. Complete eARG mineralization requires extensive backbone cleavage and oxidation of bases to low-molecular-weight products and inorganic N/P species; this is a demanding endpoint and may require substantial photon, oxidant, or electrical energy when pursued in real matrices. Moreover, photocatalytic lysis of dead or injured ARB can continuously release new eARGs during treatment, while eARGs may adsorb onto cell debris, suspended solids, or biofilms where they are partly shielded from ROS. Therefore, eARG destruction is governed not only by radical yield but also by interfacial residence time, target renewal through cell lysis, and the accessibility of DNA bound to solids [46, 55, 98].

Multiple complementary analytical and material-design strategies are needed. Transformation assays using competent bacteria should verify loss of biological function; long-amplicon qPCR, dPCR, or sequencing can better resolve fragmentation; and LC–MS/HRMS product analysis, TOC/DOC loss, and phosphate/nitrogen release can provide stronger evidence of mineralization [51, 60, 99]. From a design perspective, eARG-focused studies should prioritize strong but regenerable DNA adsorption, high local $^{\bullet}OH$ or direct-hole flux, and evaluation of energy-normalized mineralization rather than reporting qPCR loss alone [100].

6.2 | ROS Scavenging and Target Shielding in Realistic Matrices

The treatment of ARGs in real wastewater matrices is fundamentally constrained by competitive reaction environments. Dissolved organic matter (DOM; typically, 5–50 mg L^{-1} as TOC), bicarbonate/carbonate (1–10 mM), and other background constituents are present at concentrations orders of magnitude higher than extracellular ARGs (often ng–μg L^{-1}). These species act as effective ROS scavengers, with second-order rate constants for •OH typically in the range of 10^6–10^9 $M^{-1}s^{-1}$, thereby rapidly consuming reactive species before they interact with target DNA [23, 101, 102]. The challenge in treating ARGs in real wastewater matrices is significant and this complexity often leads to an overestimation of treatment efficacy when studies are conducted using clean matrices.

To overcome these matrix-induced limitations, future research should prioritize systematic evaluation of photocatalytic performance in real wastewater and effluent matrices to capture competitive kinetics and radical scavenging effects [101, 103]. Advanced material strategies are required to shift from bulk diffusion-limited reactions toward interfacial, target-selective processes, which include developing molecular imprinting strategies that selectively bind ARGs while excluding scavengers [46, 104], utilizing nanoconfinement to create local environments where target concentration exceeds scavenger concentration [105], and designing materials that generate ROS through pathways less susceptible to DOM quenching like direct h^+ transfer [106, 107].

6.3 | Catalyst Fouling, Regeneration and Biofilm Risk

Adsorption of ARB/ARGs onto photocatalysts is mechanistically beneficial because it shortens transport distances, but it can also shorten the operational lifetime of the catalyst. Bacterial cells, lysed-cell residues, proteins, extracellular polymeric substances, and adsorbed DNA can mask active sites, attenuate light penetration, consume ROS nonselectively, and alter surface charge. In authentic wastewater, incomplete removal of these residues may provide conditioning films that promote subsequent microbial attachment and biofilm development [48, 52, 53]. Therefore, photocatalytic disinfection should be evaluated over repeated cycles using activity retention, surface fouling markers, zeta-potential drift, photocurrent/PL changes, ROS yield, metal leaching, and microscopy of residual biomass rather than single-cycle inactivation alone.

Regeneration strategies should be built into reactor design. Practical options include immobilized or magnetic photocatalysts to enable separation, hydraulic backwashing or shear-assisted cleaning, mild alkaline or oxidant washing, periodic photo-regeneration, membrane-photocatalyst configurations with controllable cleaning cycles and pretreatment to reduce particulate/organic loading [108–112]. The key requirement is to preserve the target-capture function while preventing irreversible coverage of reactive sites and minimizing secondary nanoparticle release.

6.4 | Irreversible Killing Thresholds, Dormancy and Post-Treatment Regrowth

Microorganisms differ from conventional chemical pollutants because sublethally injured cells can repair membranes and DNA, enter viable-but-nonculturable or persister-like states, and later regrow under favorable conditions [48, 49]. A reported 4–6 log CFU reduction can satisfy practical disinfection benchmarks, but it does not by itself prove that dormant, VBNC or biofilm-associated subpopulations have been eliminated. The operational threshold for photocatalytic ARB control should therefore be defined by combined evidence: sustained CFU loss, reduced intact-cell counts, loss of metabolic activity, absence of regrowth over 24–72 h under nutrient-rich and matrix-relevant conditions, decreased PMA-qPCR signal for intracellular ARGs and reduced transformation/conjugation potential [14, 48, 50, 51, 60, 99, 100, 107]. Such multi-endpoint validation helps distinguish irreversible killing from temporary growth arrest or repairable oxidative injury.

6.5 | Sustainability Blind Spot in Photocatalytic Systems

Despite significant advances in photocatalytic configurations, sustainability considerations remain a critical blind spot limiting large scale implementation. The synthesis of many highly efficient photocatalysts often involves energy-intensive processes, the use of scarce or noble metals, and hazardous reagents, all of which contribute to elevated environmental footprints and production costs, resulting in significant environmental and economic challenges to their practical application. Life cycle assessment (LCA) evaluates the environmental impacts of these processes; however, it is underutilized in the field of photocatalysis. Additionally, the leaching of metal ions or nanoparticles remains insufficiently addressed, raising concerns regarding secondary contamination and long-term ecological risks [113, 114].

To overcome these critical challenges, sustainability must be embedded at the materials design stage. This includes integrating LCA from early development stages, comparing energy demand, material toxicity, and end-of-life scenarios [114–117], favoring the use of earth-abundant elements (Fe, Cu, Mn, C, N) over noble metals [118, 119], selective recovery of precious metals [120, 121], and developing magnetic or immobilization techniques for catalyst recovery and reuse [108, 109]. Collectively, integrating sustainability metrics with photocatalytic performance is essential to transition from laboratory-scale innovation to environmentally responsible, real-world water treatment applications.

7 | Emerging Frontiers: Demonstrated Tools and Prospective Directions

7.1 | Selective Nanomaterials

Among various selective nanomaterials, molecularly imprinted photocatalysts represent the most clearly demonstrated method for targeting ARGs. MIPs form recognition cavities that concentrate target DNA sequences near oxidizing sites, thereby shifting degradation from indiscriminate bulk oxidation to a more targeted interfacial attack [46, 122]. For instance, molecularly imprinted graphitic carbon nitride (MIP-C_3N_4) has been shown to accelerate degradation of blaNDM-1 compared to non-imprinted counterparts, indicating that adsorption informed by the sequence can enhance eARG photodegradation [46]. This method is thus an experimentally validated, short-term strategy, although its effectiveness in high-DOM wastewater and mixed ARG environments still needs confirmation.

In contrast, CRISPR-coupled photocatalytic treatment should be viewed as a conceptual idea rather than a fully developed ARB/ARG photocatalysis platform. CRISPR/Cas systems, such as Cas12a, have shown high sequence specificity for detecting and cleaving ARGs in molecular assays, and nanoparticle carriers have been suggested to improve delivery [123–126]. However, challenges remain in achieving stable delivery into diverse wastewater bacterial communities, avoiding unintended ecological impacts, integrating catalysts, and ensuring biosafety. Therefore, we propose CRISPR-assisted materials as a promising direction for selective ARG recognition, rather than as a fully mature treatment technology.

7.2 | Integrated Platforms

7.2.1 | Photocatalytic Membrane

Membrane photoreactors combine physical separation with in situ ROS generation, providing superior water treatment by integrating size exclusion for antibiotic-resistant bacteria/particulates and photocatalytic degradation. They leverage pore confinement for high-concentration ROS, electrostatic repulsion for anionic ARGs, and photocatalytic oxidation to reduce biofouling, enhance efficiency and minimize operational challenges [111, 112]. Light-responsive self-cleaning membranes represent the state of the art in photocatalytic water treatment. Hou et al. [110] fabricated a TA@Fe-TiO_2/PVDF membrane by depositing a tannic acid–iron complex onto PVDF, integrating photothermal activation (TA@Fe) with photocatalysis (TiO_2) to achieve nearly 100% bactericidal efficiency and 98% ARG removal. Figure 8a–h demonstrates that a thin photocatalytic coating generates $^{\bullet}OH$ and $^1O_2$ while locally elevating surface temperature under irradiation, forming a confined oxidative interface. As mechanistically illustrated in Figure 8i–k, dual Fe/Ti active sites enhance oxygen adsorption and interfacial electron transfer, promoting localized ROS production. Filtration-induced pollutant accumulation restricts reactions to the boundary layer, enabling the membrane to function as a continuous-flow microreactor for in situ degradation of bacteria and ARGs. The narrowed pore channels served as microreactors in PVDF ultrafiltration membranes, increasing local ROS concentration and collision probability while reducing diffusion distances to targets [112].

7.2.2 | Photocatalysis-Fenton Hybrid Systems

Coupling photocatalysis with Fenton chemistry (photo-Fenton) overcomes individual limitations by using photo-generated electrons to accelerate Fe^{3+}/Fe^{2+} cycling, enhancing H_2O_2 decomposition into $^{\bullet}OH$. The synergy improves mineralization rates, reduces iron sludges and expands operational pH ranges [25, 127]. Photocatalysis–Fenton hybrid systems operate through interfacial redox synergy, where photogenerated charge carriers sustain catalytic iron cycling [87]. As shown in Figure 9a–c, photoexcited electrons from Bi_2WO_6 migrate to FeOOH, reducing Fe^{3+} to Fe^{2+} and continuously activating H_2O_2 to generate $^{\bullet}OH$ radicals, while holes and $O_2^{\bullet-}$ originate from photocatalytic pathways. Figure 9d further reveals that Fermi-level equilibration creates a built-in electric field that directs carrier migration and suppresses recombination. This coupling integrates photocatalytic oxidation with Fenton chemistry into a closed redox loop, enabling simultaneous ROS amplification and efficient Fe(III)/Fe(II) regeneration. The result is enhanced antibiotic degradation and ARB inactivation beyond either process alone [87]. Furthermore, bimetallic Fe-Cu systems exploit synergistic redox cycles. The Fe^{3+}/Fe^{2+} and Cu^{2+}/Cu^{+} cycles operate cooperatively, where Cu^{+} reduces Fe^{3+} to Fe^{2+}, accelerating Fenton chemistry while photocatalysis regenerates both reduced species [127].

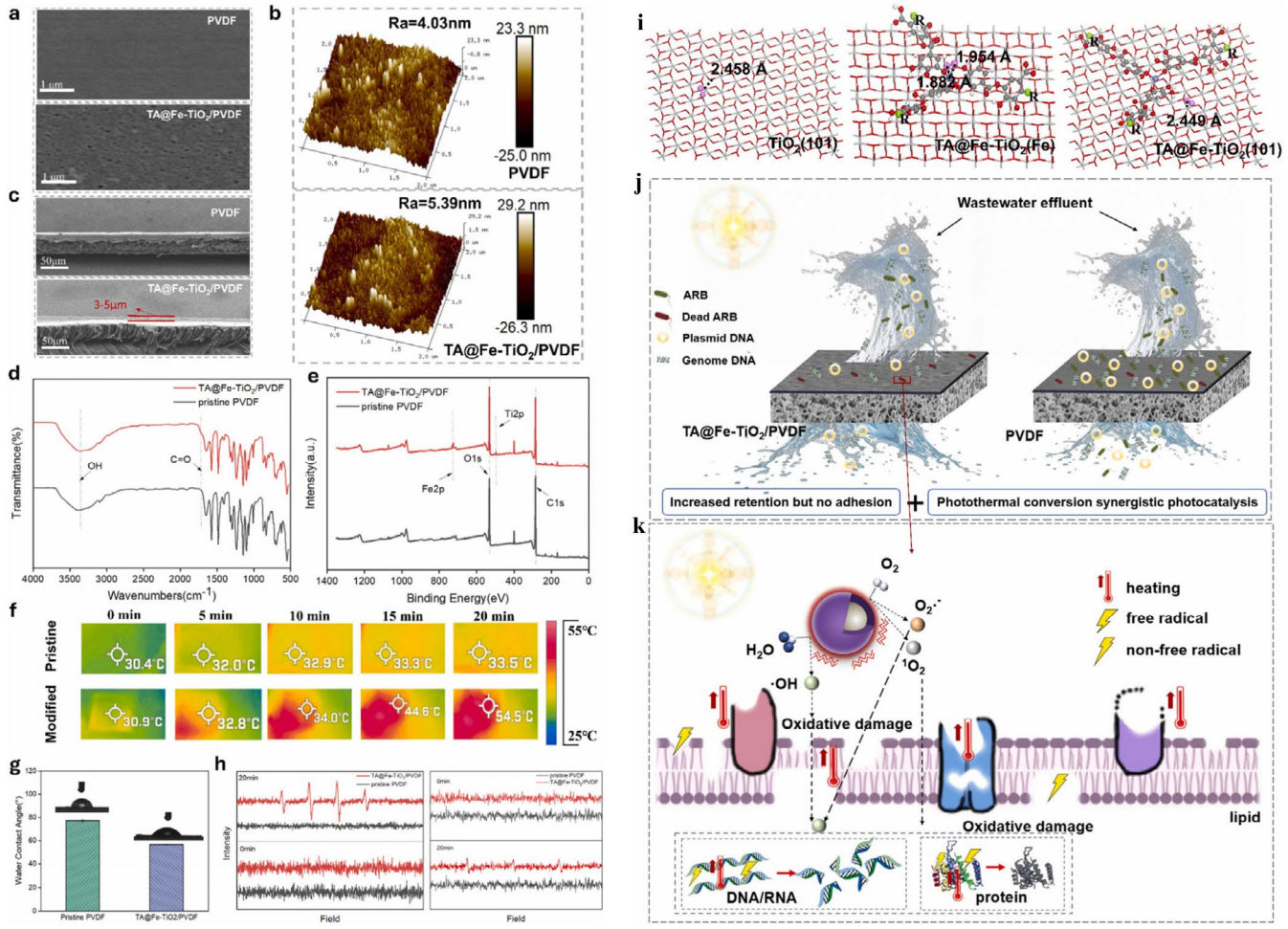

FIGURE 8 | Light-responsive TA@Fe-TiO_2/PVDF photocatalytic membrane enabling confined interfacial oxidation. (a–c) Morphology and cross-sectional structure showing formation of a ~3–5 μm catalytic layer on PVDF. (d, e) FTIR and XPS confirming surface functionalization. (f) Infrared imaging showing localized photothermal heating. (g, h) Enhanced hydrophilicity and in situ ROS generation ($^{\bullet}OH$, $^1O_2$). (i) DFT analysis indicating improved O_2 adsorption at Fe/Ti sites. (j, k) Schematic illustration of filtration-assisted pollutant retention and synergistic photothermal–photocatalytic oxidation leading to bacterial and ARG degradation at the membrane interface. Reprinted with permission from [110]. Copyright 2024, Elsevier.

7.2.3 | Photocatalysis-Constructed Wetlands

Constructed wetlands (CWs) provide low-energy and sustainable wastewater treatment but typically achieve limited antibiotic resistance genes removal (< 1-log) due to reliance on passive adsorption and biodegradation [128]. Integrating photocatalysis fundamentally enhances performance of CWs. Chen et al. [129] compared three CWs configurations, series photocatalysis-CW (S-PT-CW), built-in photocatalysis-CW (B-PT-CW), and conventional CW (S-CW) (Figure 10a–c). B-PT-CW achieved the highest intracellular ARGs removal (1.27–1.72 log) via substrate adsorption and plant–microbial uptake, whereas S-PT-CW maximized extracellular ARGs degradation (0.23–0.65 log) through photocatalytic oxidation (Figure 10d–g). Photocatalysis further reshaped microbial communities, enriching denitrifying Proteobacteria and phosphorus-accumulating taxa. The hybrid system therefore establishes a functional division of labor: wetlands remove protected intracellular genes, while photocatalysis oxidizes extracellular DNA and suppresses host bacteria, enabling sustained ARG attenuation.

7.3 | Machine Learning-Guided Design

Machine learning (ML) represents another emerging frontier, although current findings should be interpreted carefully. ML has already been applied to predict band structures, defect descriptors, surface properties, and photocatalytic activity in broader photocatalyst discovery, whereas direct ARB/ARGs-specific datasets remain limited [130–135]. Therefore, ML-guided design for antibiotic resistance control should presently be viewed as a data integration and hypothesis generation tool rather than a fully validated replacement for matrix-specific experiments.

The most realistic near-term application is to integrate curated literature data, high-throughput synthesis and characterization, physics informed descriptors, including band positions, ROS yield, surface charge, adsorption constants, pore accessibility, light distribution, and matrix scavenging capacity. Such models could help screen candidate materials for target specific interfaces and prioritize experiments under realistic wastewater conditions.

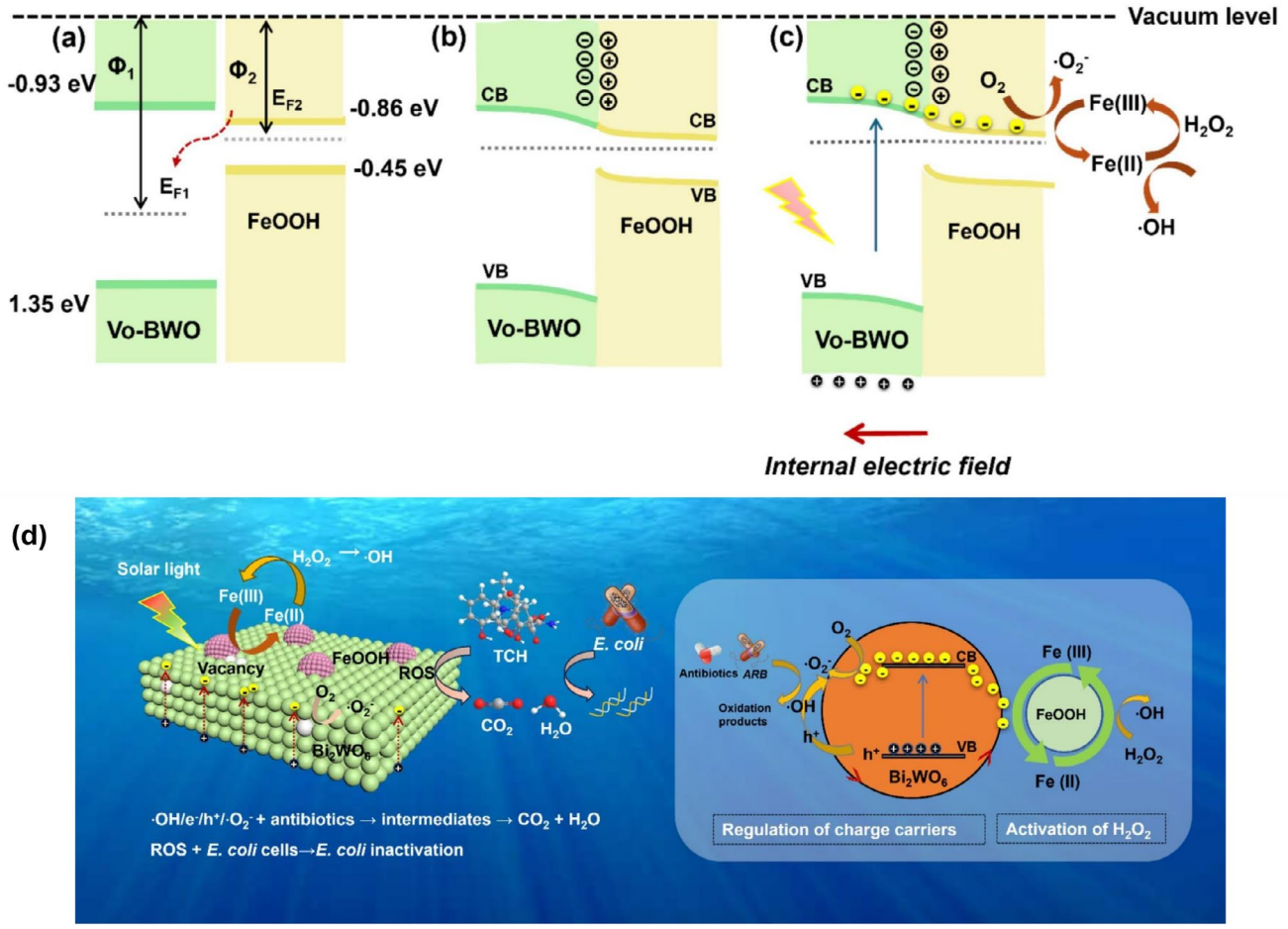

FIGURE 9 | Charge transfer pathways and inactivation mechanism: Energy band arrangements of Vo-BWO and FeOOH (a) before contact; (b) after contact in darkness; (c) contact under illumination; and (d) Schematic illustration of the integrated photo-Fenton process showing vacancy-assisted charge transport, ROS generation, antibiotic degradation, and multidrug-resistant *E. coli* inactivation. Reprinted with permission from [87]. Copyright 2025, Elsevier.

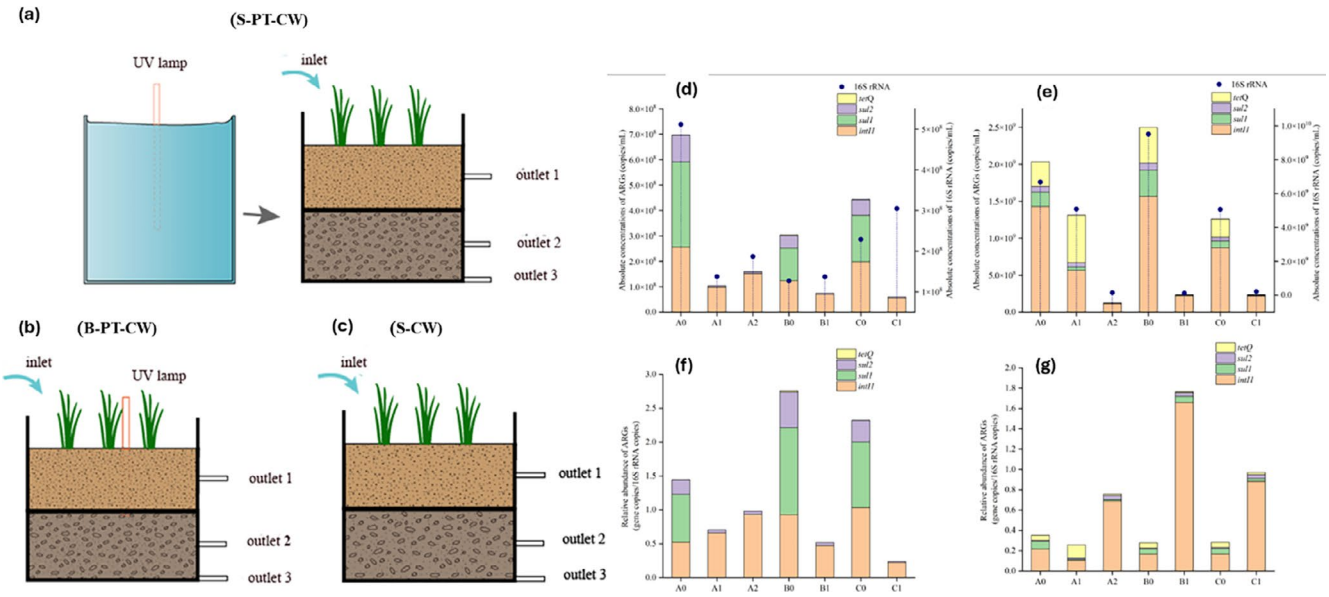

FIGURE 10 | Configurations and performance of photocatalysis–constructed wetland hybrids. (a–c) Constructed wetland system designs (S-PT-CW, B-PT-CW, and S-CW). (d, e) Absolute ARGs abundances during treatment. (f, g) Relative ARGs distribution. Reprinted with permission from [129]. Copyright 2023, Elsevier.

Adjacent demonstration in high-throughput photocatalysis, MXene bandgap prediction, metal oxide screening show how automated synthesis and ML-assisted analysis can accelerate materials discovery [133–137]. However, these studies do not yet provide direct evidence of ARB/ARGs photocatalytic treatment performance. Future models should therefore include standardized biological endpoints, regrowth data, eARG transformation assays, and energy-normalized metrics to avoid optimizing only apparent qPCR removal or dye-degradation proxies.

8 | Conclusion

The photocatalytic control of antibiotic resistance has progressed from empirical material discovery to rational interfacial engineering. This review has advanced a paradigm centered on the interfacial battlefield, where surface charge dictates target adsorption, charge separation determines ROS generation pathways, and nanoconfinement concentrates oxidative attack within the diffusion radius of short-lived $^{\bullet}OH$. The reaction–diffusion framework provides a quantitative foundation for this paradigm, demonstrating through Damköhler analysis that photocatalytic ARB/ARG destruction operates in transport-limited regimes ($Da \gg 1$) where adsorption kinetics and interfacial residence time govern overall efficiency. This mechanistic insight explains why materials with strong target affinity often outperform those with higher intrinsic ROS generation but poor adsorption. The following key principles have emerged:

1. ARB and ARGs require distinct strategies. Live bacterial cells require membrane disruption and intracellular ROS penetration; whereas eARGs demand adsorption and high-potential surface oxidation.
2. Z-scheme and S-scheme heterojunctions preserve high redox potential while maintaining charge separation, outperforming conventional Type-II designs.
3. Oxygen vacancies and other defects serve dual functions: extending light absorption and creating reactive hotspots for co-catalyst activation.
4. Conductive carbon architectures function as electron highways, extracting charges and enabling multi-electron reduction pathways.
5. Integrated platforms—photocatalytic membranes, hybrid Fenton systems, constructed wetlands—exploit synergistic mechanisms and offer practical scalability.
6. Emerging frontiers as novel paths for advancing photocatalysis. Selective nanomaterials target specific ARGs while machine learning-guided design facilitates high throughput automated screening and optimizing materials.

Despite great advances in interfacial photocatalysis, significant gaps persist in mitigation of antibiotic resistance. The reaction–diffusion framework reveals that complete eARG mineralization requires not merely adsorption but sufficient interfacial residence time ($\tau_{res} = 1/k_{des}$) for cumulative $^{\bullet}OH$ attack, a condition rarely verified in current studies. Complete eARGs mineralization is unproven, matrix effects are underexplored, standardization is absent, and sustainability is overlooked. Addressing these challenges requires a concerted shift from descriptive cataloging to hypothesis-driven, mechanism-focused research. By centering design on the photocatalytic interface and embracing rigorous, real-world validation, the field can finally transform laboratory potential into scalable solutions against the escalating threat of antibiotic resistance.

Author Contributions

Rajendra Singh: conceptualization, investigation, literature review, writing – original draft preparation. **Jin Chul Joo:** formal analysis, visualization, writing – original draft preparation, writing – review and editing. **Keugtae Kim:** formal analysis, visualization, resources, project administration, writing – review and editing.

Acknowledgments

This work was supported by Korea Environment Industry & Technology Institute (KEITI) through Technology development project to optimize planning, operation, and maintenance of urban flood control facilities, funded by Korea Ministry of Environment (MOE) (RS-2024-00398012).

Funding

The work was supported by the Korea Ministry of Environment (MOE) (RS-2024-00398012).

Conflicts of Interest

The authors declare no conflicts of interest.

Data Availability Statement

The data that support the findings of this study are available from the corresponding author upon reasonable request.

References

1. Wellspect, "Do You Know That Antibiotic Resistance Is Also Called a Silent Pandemic?" (2024), https://www.wellspect.us/education/articles/antibiotic-resistance-the-silent-pandemic/.

2. T. V. A. Gavi, "The Silent Pandemic of Antibiotic Resistance," (2021), https://www.gavi.org/vaccineswork/silent-pandemic-antibiotic-resistance?gad_source=1&gad_campaignid=12319817265&gbraid=0AAAADibICMd57eiLzLUwMiYk13mhLvO3&gclid=CjwKCAiA2PrMBhA4EiwAwpHyCwjQurNQERR6e1GjjhSk1cUnPuoMHy4hto8pWAvnIFJ8hBdrphsmyRoCwJcQAvD_BwE.

3. WHO, *Global Antibiotic Resistance Surveillance Report 2025: WHO Global Antimicrobial Resistance and Use Surveillance System (GLASS)* (World Health Organization, 2025). Licence: CC BY-NC-SA 3.0 IGO.

4. G. Reina, D. Panáček, K. Rathammer, et al., "Light Irradiation of N-Doped Graphene Acid: Metal-Free Strategy Toward Antibacterial and Antiviral Coatings With Dual Modes of Action," *EcoMat* 7, no. 4 (2025): e70009, https://doi.org/10.1002/eom2.70009.

5. C. J. Murray, K. S. Ikuta, F. Sharara, et al., "Global Burden of Bacterial Antimicrobial Resistance in 2019: A Systematic Analysis," *Lancet* 399, no. 10325 (2022): 629–655, https://doi.org/10.1016/S0140-6736(21)02724-0.

6. O. B. Jonas, A. Irwin, F. C. J. Berthe, F. G. Le Gall, and P. V. Marquez, *Drug-Resistant Infections: A Threat to Our Economic Future* (World Bank Group, 2017), 1–132.

7. X. Cong, P. Mazierski, M. Miodyńska, et al., "The Role of TiO_2 and gC_3N_4 Bimetallic Catalysts in Boosting Antibiotic Resistance Gene Removal Through Photocatalyst Assisted Peroxone Process," *Scientific*

Reports 14, no. 1 (2024): 22897, https://doi.org/10.1038/s41598-024-74147-4.

8. J. S. Cedeño-Muñoz, S. A. Aransiola, K. V. Reddy, et al., "Antibiotic Resistant Bacteria and Antibiotic Resistance Genes as Contaminants of Emerging Concern: Occurrences, Impacts, Mitigations and Future Guidelines," *Science of the Total Environment* 952 (2024): 175906, https://doi.org/10.1016/j.scitotenv.2024.175906.

9. J. M. Sousa, G. Macedo, M. Pedrosa, et al., "Ozonation and UV254 Nm Radiation for the Removal of Microorganisms and Antibiotic Resistance Genes From Urban Wastewater," *Journal of Hazardous Materials* 323 (2017): 434–441, https://doi.org/10.1016/j.jhazmat.2016.03.096.

10. P. Cheng, B. Wang, Q. Ji, et al., "Fe-Doped TiO_2 Nanosheet Exposure Accelerates the Spread of Antibiotic Resistance Genes by Promoting Plasmid-Mediated Conjugative Transfer," *Journal of Hazardous Materials* 490 (2025): 137715, https://doi.org/10.1016/j.jhazmat.2025.137715.

11. H. Yu, X. Zhang, J. Zhao, T. Sun, and Y. Zhu, "Mechanism of TiO_2 Nanotube UV-Photocatalytic Degradation of Antibiotic Resistance Genes in the Wastewater Sludge and Blocking of the Transfer," *Frontiers in Environmental Science* 13 (2025): 1590101, https://doi.org/10.3389/fenvs.2025.1590101.

12. J. Ji, Y. Bao, X. Liu, J. Zhang, and M. Xing, "Molybdenum-Based Heterogeneous Catalysts for the Control of Environmental Pollutants," *EcoMat* 3, no. 6 (2021): e12155, https://doi.org/10.1002/eom2.12155.

13. Y. Shu, Y. Zhao, X. Linghu, et al., "NaGdF4:Yb,Er@ZIF-8/MnO_2 for Photocatalytic Removal of Organic Pollutants and Pathogenic Bacteria," *EcoMat* 6, no. 1 (2024): e12427, https://doi.org/10.1002/eom2.12427.

14. Y. Ahmed, J. Lu, Z. G. Yuan, P. L. Bond, and J. H. Guo, "Efficient Inactivation of Antibiotic Resistant Bacteria and Antibiotic Resistance Genes by Photo-Fenton Process Under Visible LED Light and Neutral pH," *Water Research* 179 (2020): 115878, https://doi.org/10.1016/j.watres.2020.115878.

15. B. R. Gao, M. M. Dou, J. Wang, et al., "Efficient Persulfate Activation by Carbon Defects g-C3N4 Containing Electron Traps for the Removal of Antibiotics, Resistant Bacteria and Genes," *Chemical Engineering Journal* 426 (2021): 131677, https://doi.org/10.1016/j.cej.2021.131677.

16. R. Gao, S. H. Gao, J. Li, et al., "Emerging Technologies for the Control of Biological Contaminants in Water Treatment: A Critical Review," *Engineering* 48 (2025): 185–204, https://doi.org/10.1016/j.eng.2024.08.022.

17. F. Li, K. W. Liu, Y. P. Bao, et al., "Molecular Level Removal of Antibiotic Resistant Bacteria and Genes: A Review of Interfacial Chemical in Advanced Oxidation Processes," *Water Research* 254 (2024): 121373, https://doi.org/10.1016/j.watres.2024.121373.

18. A. Mukherjee, S. Das, and Y.-H. Ahn, "Synergistic Effect of Sono-Photocatalysis With Blue LED and Natural Photosensitizer Terpinolene for Rapid Disinfection of Multi-Drug Resistant Coliform Bacteria in Wastewater," *Journal of Water Process Engineering* 49 (2022): 103186, https://doi.org/10.1016/j.jwpe.2022.103186.

19. V. K. Sharma, N. Johnson, L. Cizmas, T. J. McDonald, and H. Kim, "A Review of the Influence of Treatment Strategies on Antibiotic Resistant Bacteria and Antibiotic Resistance Genes," *Chemosphere* 150 (2016): 702–714, https://doi.org/10.1016/j.chemosphere.2015.12.084.

20. O. Baaloudj, I. Assadi, N. Nasrallah, A. El Jery, L. Khezami, and A. A. Assadi, "Simultaneous Removal of Antibiotics and Inactivation of Antibiotic-Resistant Bacteria by Photocatalysis: A Review," *Journal of Water Process Engineering* 42 (2021): 102089, https://doi.org/10.1016/j.jwpe.2021.102089.

21. P. Karaolia, I. Michael-Kordatou, E. Hapeshi, et al., "Removal of Antibiotics, Antibiotic-Resistant Bacteria and Their Associated Genes by Graphene-Based TiO_2 Composite Photocatalysts Under Solar Radiation in Urban Wastewaters," *Applied Catalysis B: Environmental* 224 (2018): 810–824, https://doi.org/10.1016/j.apcatb.2017.11.020.

22. D. Saha, M. C. Visconti, M. M. Desipio, and R. Thorpe, "Inactivation of Antibiotic Resistance Gene by Ternary Nanocomposites of Carbon Nitride, Reduced Graphene Oxide and Iron Oxide Under Visible Light," *Chemical Engineering Journal* 382 (2020): 122857, https://doi.org/10.1016/j.cej.2019.122857.

23. J. X. Zhong, Y. Ahmed, G. Carvalho, et al., "Simultaneous Removal of Micropollutants, Antibiotic Resistant Bacteria, and Antibiotic Resistance Genes Using Graphitic Carbon Nitride Under Simulated Solar Irradiation," *Chemical Engineering Journal* 433 (2022): 133839, https://doi.org/10.1016/j.cej.2021.133839.

24. J. Ye, A. M. Beagan, S.-R. Guo, A. Hayat, and Y. Orooji, "Synergistic Effects in Copolymerized Carbon Nitride/MoO_3 Heterojunction Composites for Efficient Visible-Light-Driven Photocatalysis," *EcoMat* 7, no. 5 (2025): e70015, https://doi.org/10.1002/eom2.70015.

25. S. Giannakis, S. Watts, S. Rtimi, and C. Pulgarin, "Solar Light and the Photo-Fenton Process Against Antibiotic Resistant Bacteria in Wastewater: A Kinetic Study With a Streptomycin-Resistant Strain," *Catalysis Today* 313 (2018): 86–93, https://doi.org/10.1016/j.cattod.2017.10.033.

26. A. Basu, A. J. Misra, M. Behera, et al., "Photocatalytic Disinfection of Extended-Spectrum Beta-Lactamase Producing *Escherichia coli* Using Alumina/ZnO Heterostructures," *Journal of Environmental Chemical Engineering* 9, no. 6 (2021): 106334, https://doi.org/10.1016/j.jece.2021.106334.

27. A. Mukherjee, S. Das, and Y. H. Ahn, "Sono-Photocatalytic Disinfection of High Strength Multi-Drug Resistant Klebsiella Pneumonia in Presence of Blue LED-Active CdS Nanorods," *Journal of Environmental Chemical Engineering* 10, no. 5 (2022): 108460, https://doi.org/10.1016/j.jece.2022.108460.

28. Y. Liu, M. Xu, L. Zhao, S. He, L. Feng, and L. Wei, "Combat Against Antibiotic Resistance Genes During Photo-Treatment of Magnetic Zr-MOFs@Layered Double Hydroxide Heterojunction: Conjugative Transfer Risk Mitigating and Bacterial Inactivation," *Journal of Hazardous Materials* 492 (2025): 138160, https://doi.org/10.1016/j.jhazmat.2025.138160.

29. Y. Liu, M. Xu, W. Zhao, et al., "Interfacial Architecture on Quantum Dots Modified Metal-Organic Frameworks: Charge Transfer Mechanism, Antibiotic Associated Pollutants Photodegradation and Eco-Toxicity Prediction," *Water Research* 284 (2025): 123956, https://doi.org/10.1016/j.watres.2025.123956.

30. A. Ali, B. Ullah, R. Cai, et al., "COF@MXene Composites: A Paradigm Shift in Advanced Materials for Multifunctional Applications in Energy, Environmental Protection, and Catalysis," *EcoMat* 7, no. 11 (2025): e70036, https://doi.org/10.1002/eom2.70036.

31. J. Zhong, Y. Ahmed, Z. Yu, J. F. Mueller, and J. Guo, "Synergistic Combination of Graphitic Carbon Nitride and Peroxymonosulfate for Efficient Photocatalytic Destruction of Emerging Contaminants Under Simulated Solar Irradiation," *ACS ES&T Water* 3, no. 1 (2023): 6–15, https://doi.org/10.1021/acsestwater.2c00237.

32. X. Chen, W. Han, M. Patel, et al., "Inactivation of a Pathogenic NDM-1-Positive *Escherichia coli* Strain and the Resistance Gene blaNDM-1 by TiO2/UVA Photocatalysis," *Science of the Total Environment* 846 (2022): 157369, https://doi.org/10.1016/j.scitotenv.2022.157369.

33. A. P. V. Ferreyra Maillard, J. C. Espeche, P. Maturana, A. C. Cutro, and A. Hollmann, "Zeta Potential Beyond Materials Science: Applications to Bacterial Systems and to the Development of Novel Antimicrobials," *Biochimica et Biophysica Acta (BBA) - Biomembranes* 1863, no. 6 (2021): 183597, https://doi.org/10.1016/j.bbamem.2021.183597.

34. F. C. Neuhaus and J. Baddiley, "A Continuum of Anionic Charge: Structures and Functions of D-Alanyl-Teichoic Acids in Gram-Positive Bacteria," *Microbiology and Molecular Biology Reviews* 67, no. 4 (2003): 686–723, https://doi.org/10.1128/mmbr.67.4.686-723.2003.

35. H. Nikaido, "Molecular Basis of Bacterial Outer Membrane Permeability Revisited," *Microbiology and Molecular Biology Reviews* 67, no. 4 (2003): 593–656, https://doi.org/10.1128/mmbr.67.4.593-656.2003.

36. T. J. Silhavy, D. Kahne, and S. Walker, "The Bacterial Cell Envelope," *Cold Spring Harbor Perspectives in Biology* 2, no. 5 (2010): a000414, https://doi.org/10.1101/cshperspect.a000414.

37. L. Wang, J. C. Zhou, Z. H. Li, et al., "Facet-Specific Photocatalytic Degradation of Extracellular Antibiotic Resistance Genes by Hematite Nanoparticles in Aquatic Environments," *Environmental Science and Technology* 57, no. 51 (2023): 21835–21845, https://doi.org/10.1021/acs.est.3c06571.

38. W. W. Wilson, M. M. Wade, S. C. Holman, and F. R. Champlin, "Status of Methods for Assessing Bacterial Cell Surface Charge Properties Based on Zeta Potential Measurements," *Journal of Microbiological Methods* 43, no. 3 (2001): 153–164, https://doi.org/10.1016/S0167-7012(00)00224-4.

39. M. Yu, D. Liu, L. Wang, et al., "A Zn-Al-Zr Layered Double Hydroxide/Graphene Oxide Nanocomposite Enables Rapid Photocatalytic Removal of Kanamycin-Resistance Bacteria and Genes via Nano-Confinement Effects," *Applied Catalysis B: Environmental* 350 (2024): 123922, https://doi.org/10.1016/j.apcatb.2024.123922.

40. M. Zhuang, Y. Achmon, Y. Cao, et al., "Distribution of Antibiotic Resistance Genes in the Environment," *Environmental Pollution* 285 (2021): 117402, https://doi.org/10.1016/j.envpol.2021.117402.

41. B. Ran, L. Ran, Z. Wang, et al., "Photocatalytic Antimicrobials: Principles, Design Strategies, and Applications," *Chemical Reviews* 123, no. 22 (2023): 12371–12430, https://doi.org/10.1021/acs.chemrev.3c00326.

42. X. Zhang, M. C. Yao, L. Chen, and G. P. Sheng, "Lewis Acid-Base Interaction Triggering Electron Delocalization to Enhance the Photodegradation of Extracellular Antibiotic Resistance Genes Adsorbed on Clay Minerals," *Environmental Science & Technology* 56, no. 24 (2022): 17684–17693, https://doi.org/10.1021/acs.est.2c05785.

43. S. Baker, G. R. Elliott, E. J. Wanless, G. B. Webber, V. S. J. Craig, and A. J. Page, "A Multimodal Screening Length Analysis of Concentrated Electrolytes," *Journal of Colloid and Interface Science* 709 (2026): 139953, https://doi.org/10.1016/j.jcis.2026.139953.

44. M. Gmurek, J. Alexander, P. Mazierski, et al., "Enhancement of Photocatalytic-Based Processes by Mono- and Bimetallic (CuPd) Rutile Loaded Nanoparticles for Antibiotic Resistance Genes and Facultative Pathogenic Bacteria Removal," *Chemical Engineering Journal* 462 (2023): 142243, https://doi.org/10.1016/j.cej.2023.142243.

45. B. T. Psciuk, R. L. Lord, B. H. Munk, and H. B. Schlegel, "Theoretical Determination of One-Electron Oxidation Potentials for Nucleic Acid Bases," *Journal of Chemical Theory and Computation* 8, no. 12 (2012): 5107–5123, https://doi.org/10.1021/ct300550x.

46. Q. Yuan, D. Zhang, P. Yu, et al., "Selective Adsorption and Photocatalytic Degradation of Extracellular Antibiotic Resistance Genes by Molecularly-Imprinted Graphitic Carbon Nitride," *Environmental Science and Technology* 54, no. 7 (2020): 4621–4630, https://doi.org/10.1021/acs.est.9b06926.

47. S. Overballe-Petersen, K. Harms, L. A. A. Orlando, et al., "Bacterial Natural Transformation by Highly Fragmented and Damaged DNA," *Proceedings of the National Academy of Sciences* 110, no. 49 (2013): 19860–19865, https://doi.org/10.1073/pnas.1315278110.

48. M. Wang, M. Ateia, D. Awfa, and C. Yoshimura, "Regrowth of Bacteria After Light-Based Disinfection - What We Know and Where We Go From Here," *Chemosphere* 268 (2021): 128850, https://doi.org/10.1016/j.chemosphere.2020.128850.

49. K. Lewis, "Persister Cells, Dormancy and Infectious Disease," *Nature Reviews Microbiology* 5, no. 1 (2007): 48–56, https://doi.org/10.1038/nrmicro1557.

50. C. W. McKinney and A. Pruden, "Ultraviolet Disinfection of Antibiotic Resistant Bacteria and Their Antibiotic Resistance Genes in Water and Wastewater," *Environmental Science & Technology* 46, no. 24 (2012): 13393–13400, https://doi.org/10.1021/es303652q.

51. Y. Yoon, M. C. Dodd, and Y. Lee, "Elimination of Transforming Activity and Gene Degradation During UV and UV/H_2O_2 Treatment of Plasmid-Encoded Antibiotic Resistance Genes," *Environmental Science: Water Research & Technology* 4, no. 9 (2018): 1239–1251, https://doi.org/10.1039/C8EW00200B.

52. H. C. Flemming and J. Wingender, "The Biofilm Matrix," *Nature Reviews Microbiology* 8, no. 9 (2010): 623–633, https://doi.org/10.1038/nrmicro2415.

53. H. C. Flemming, J. Wingender, U. Szewzyk, P. Steinberg, S. A. Rice, and S. Kjelleberg, "Biofilms: An Emergent Form of Bacterial Life," *Nature Reviews Microbiology* 14, no. 9 (2016): 563–575, https://doi.org/10.1038/nrmicro.2016.94.

54. D. Tang, X. Li, L. Zhang, et al., "Reactive Oxygen Species-Mediated Signal Transduction and Utilization Strategies in Microalgae," *Bioresource Technology* 418 (2025): 132004, https://doi.org/10.1016/j.biortech.2024.132004.

55. I. Inamuddin, A. M. Asiri, and E. Lichtfouse, *Nanophotocatalysis and Environmental Applications* (Springer Nature, 2020).

56. T. Ahuja, U. Brighu, and K. Saxena, "Recent Advances in Photocatalytic Materials and Their Applications for Treatment of Wastewater: A Review," *Journal of Water Process Engineering* 53 (2023): 103759, https://doi.org/10.1016/j.jwpe.2023.103759.

57. A. Barzagan, *Photocatalytic Water and Wastewater Treatment* (IWA Publishing, 2022).

58. J. A. Imlay, "Cellular Defenses Against Superoxide and Hydrogen Peroxide," *Annual Review of Biochemistry* 77 (2008): 755–776, https://doi.org/10.1146/annurev.biochem.77.061606.161055.

59. G. Liu, Z. Hu, X. Chen, et al., "Oxygen Vacancy-Rich Ag/CuO Nanoarray Mesh Fabricated by Laser Ablation for Efficient Bacterial Inactivation," *Journal of Hazardous Materials* 465 (2024): 133269, https://doi.org/10.1016/j.jhazmat.2023.133269.

60. J. Wang, L. Huo, K. Bian, et al., "Efficacy and Mechanism of Antibiotic Resistance Gene Degradation and Cell Membrane Damage During Ultraviolet Advanced Oxidation Processes," *ACS ES&T Water* 4, no. 6 (2024): 2746–2755, https://doi.org/10.1021/acsestwater.4c00350.

61. Z. Yu, Y. Zhou, X. Liu, et al., "In3+−Doped Bi/BiOCl/Bi(In3+)-MOF Composite for Accelerating Photocatalytic Elimination of Antibiotic-Resistant Bacteria and Genes Under Co-Effect of Nanoconfinement and Reactive Oxygen Species," *Separation and Purification Technology* 361 (2025): 131318, https://doi.org/10.1016/j.seppur.2024.131318.

62. M. A. Fox and M. T. Dulay, "Heterogeneous Photocatalysis," *Chemical Reviews* 93, no. 1 (1993): 341–357, https://doi.org/10.1021/cr00017a016.

63. M. R. Hoffmann, S. T. Martin, W. Choi, and D. W. Bahnemann, "Environmental Applications of Semiconductor Photocatalysis," *Chemical Reviews* 95, no. 1 (1995): 69–96, https://doi.org/10.1021/cr00033a004.

64. A. Fujishima, X. Zhang, and D. A. Tryk, "TiO_2 Photocatalysis and Related Surface Phenomena," *Surface Science Reports* 63, no. 12 (2008): 515–582, https://doi.org/10.1016/j.surfrep.2008.10.001.

65. R. B. Bird, W. E. Stewai, and E. N. Lightfoot, *Phenomena*, Second ed. (John Wiley and Sons, 2002).

66. O. Levenspiel, *Chemical Reaction Engineering* (John Wiley & Sons, 1998).

67. M. de los Milagros Ballari, R. Brandi, O. Alfano, and A. Cassano, "Mass Transfer Limitations in Photocatalytic Reactors Employing Titanium Dioxide Suspensions: II. External and Internal Particle

Constrains for the Reaction," *Chemical Engineering Journal* 136, no. 2 (2008): 242–255, https://doi.org/10.1016/j.cej.2007.03.031.

68. P. Pichat, *Photocatalysis and Water Purification* (WILEY-VCH Verlag Gmbh & Co. kGaA, 2013).

69. J. C. Joo, C. H. Ahn, D. G. Jang, et al., "Photocatalytic Degradation of Trichloroethylene in Aqueous Phase Using Nano-ZNO/Laponite Composites," *Journal of Hazardous Materials* 263, no. Pt 2 (2013): 569–574, https://doi.org/10.1016/j.jhazmat.2013.10.017.

70. D. Monllor-Satoca, R. Gómez, M. González-Hidalgo, and P. Salvador, "The "Direct–Indirect" Model: An Alternative Kinetic Approach in Heterogeneous Photocatalysis Based on the Degree of Interaction of Dissolved Pollutant Species With the Semiconductor Surface," *Catalysis Today* 129, no. 1 (2007): 247–255, https://doi.org/10.1016/j.cattod.2007.08.002.

71. D. Li, P. Yu, X. Zhou, J. H. Kim, Y. Zhang, and P. J. J. Alvarez, "Hierarchical $Bi_2O_2CO_3$ Wrapped With Modified Graphene Oxide for Adsorption-Enhanced Photocatalytic Inactivation of Antibiotic Resistant Bacteria and Resistance Genes," *Water Research* 184 (2020): 116157, https://doi.org/10.1016/j.watres.2020.116157.

72. P. Chalatsi-Diamanti, E. A. Isari, E. Grilla, P. Kokkinos, and I. K. Kalavrouziotis, "Recent Prospects, Challenges and Advancements of Photocatalysis as a Wastewater Treatment Method," *Emerging Contaminants and Environmental Health* 4, no. 2 (2025): 12, https://doi.org/10.20517/wecn.2025.03.

73. J. G. Hedley, K. Coshic, A. Aksimentiev, and A. A. Kornyshev, "Electric Field of DNA in Solution: Who Is in Charge?," *Physical Review X* 14, no. 3 (2024): 31042, https://doi.org/10.1103/PhysRevX.14.031042.

74. W. Li, W. Li, X. Zhu, et al., "Highly Efficient Photocatalytic Elimination of Bacteria and Antibiotic Resistance Genes via a Strong Oxidation Surface in Donor-Acceptor SA-PDI@C60," *Advanced Functional Materials* 36, no. 14 (2026): e17661, https://doi.org/10.1002/adfm.202517661.

75. J. Lipfert, S. Doniach, R. Das, and D. Herschlag, "Understanding Nucleic Acid-Ion Interactions," *Annual Review of Biochemistry* 83 (2014): 813–841, https://doi.org/10.1146/annurev-biochem-060409-092720.

76. H. Ma, Y. Ding, P. Wang, and S. Zhou, "Efficient Removal for Antibiotic-Resistant Escherichia Coli and Antibiotic Resistance Genes From Aquatic Environment by BiOCl Supported Ag Quantum Dots," *Journal of Photochemistry and Photobiology A: Chemistry* 444 (2023): 114998, https://doi.org/10.1016/j.jphotochem.2023.114998.

77. Y. Hong and D. G. Brown, "Cell Surface Acid–Base Properties of *Escherichia coli* and *Bacillus brevis* and Variation as a Function of Growth Phase, Nitrogen Source and C: N Ratio," *Colloids and Surfaces B: Biointerfaces* 50, no. 2 (2006): 112–119.

78. X. Chen, W. Fu, Z. Yang, et al., "Enhanced H_2O_2 Utilization Efficiency in Fenton-Like System for Degradation of Emerging Contaminants: Oxygen Vacancy-Mediated Activation of O_2," *Water Research* 230 (2023): 119562, https://doi.org/10.1016/j.watres.2022.119562.

79. W. Gao, G. Li, Q. Wang, et al., "Ultrathin Porous Bi2WO6 With Rich Oxygen Vacancies for Promoted Adsorption-Photocatalytic Tetracycline Degradation," *Chemical Engineering Journal* 464 (2023): 142694, https://doi.org/10.1016/j.cej.2023.142694.

80. Y. Guo, W. Shi, and Y. Zhu, "Internal Electric Field Engineering for Steering Photogenerated Charge Separation and Enhancing Photoactivity," *EcoMat* 1, no. 1 (2019): e12007, https://doi.org/10.1002/eom2.12007.

81. S.-M. Lam, Z.-J. Yong, J.-C. Sin, et al., "Improved Photoelectrochemical Activity of $NiFe_2O_4/Bi_2WO_6$ Photoanode by ZnO Nanorod Array Layer for Bifunctional Photocatalytic Fuel Cell," *Applied Surface Science* 691 (2025): 162702, https://doi.org/10.1016/j.apsusc.2025.162702.

82. F. Liu, Y. Hou, S. Wang, Z. Li, B. Zhang, and M. Tong, "Periodate Activation by Pyrite for the Disinfection of Antibiotic-Resistant Bacteria: Performance and Mechanisms," *Water Research* 230 (2023): 119508, https://doi.org/10.1016/j.watres.2022.119508.

83. J. Low, J. Yu, M. Jaroniec, S. Wageh, and A. A. Al-Ghamdi, "Heterojunction Photocatalysts," *Advanced Materials* 29, no. 20 (2017): 1601694, https://doi.org/10.1002/adma.201601694.

84. J. Mohammed, E. R. Elsharkawy, S. M. El-Bahy, et al., "Z-Scheme and S-Scheme Heterostructured Photocatalyst for Photocatalytic Water Splitting: A Review Towards Efficient H_2 Generation," *Materials Today Sustainability* 32 (2025): 101227, https://doi.org/10.1016/j.mtsust.2025.101227.

85. K. Pournemati and A. Habibi-Yangjeh, "Recent Insights on Z-Scheme and S-Scheme Photocatalysts for Nitrogen Conversion to Ammonia: A Review," *Materials Today Sustainability* 28 (2024): 101043, https://doi.org/10.1016/j.mtsust.2024.101043.

86. L. Wang, X. Huang, M. Han, et al., "Efficient Inhibition of Photogenerated Electron-Hole Recombination Through Persulfate Activation and Dual-Pathway Degradation of Micropollutants Over Iron Molybdate," *Applied Catalysis B: Environmental* 257 (2019): 117904, https://doi.org/10.1016/j.apcatb.2019.117904.

87. Q. Wang, R. F. Zhao, H. R. Li, et al., "Oxygen Vacancy-Mediated Bi_2WO_6/FeOOH Heterojunction for Efficient Photo-Fenton Degradation Antibiotics and Synergistic Sterilization," *Separation and Purification Technology* 359 (2025): 130546, https://doi.org/10.1016/j.seppur.2024.130546.

88. Z. Wang and L. Wang, "Role of Oxygen Vacancy in Metal Oxide Based Photoelectrochemical Water Splitting," *EcoMat* 3, no. 1 (2021): e12075, https://doi.org/10.1002/eom2.12075.

89. Q. Xu, L. Zhang, B. Cheng, J. Fan, and J. Yu, "S-Scheme Heterojunction Photocatalyst," *Chem* 6, no. 7 (2020): 1543–1559, https://doi.org/10.1016/j.chempr.2020.06.010.

90. J. Yuan, H. Li, G. Wang, et al., "Adsorption, Isolated Electron/Hole Transport, and Confined Catalysis Coupling to Enhance the Photocatalytic Degradation Performance," *Applied Catalysis B: Environmental* 303 (2022): 120892, https://doi.org/10.1016/j.apcatb.2021.120892.

91. X. Du, I. Skachko, A. Barker, and E. Y. Andrei, "Approaching Ballistic Transport in Suspended Graphene," *Nature Nanotechnology* 3, no. 8 (2008): 491–495, https://doi.org/10.1038/nnano.2008.199.

92. E. Ilkhas, A. A. Babaei, L. Roomiani, R. J. Yengejeh, and K. Varshosaz, "Enhancing Aquaculture Management: Utilizing Cu-Doped ZnO/Graphene Nanocomposite for Effective Reduction of Antibiotics and Antibiotic-Resistant Bacteria in Shrimp Culturing Ponds," *Aquaculture* 586 (2024): 740797, https://doi.org/10.1016/j.aquaculture.2024.740797.

93. H. Jin, W. Zhou, Z. Guo, et al., "Consolidating CQDs With NiFe-MOF Photo-Fenton Membranes to Effectively Treat Wastewater Containing Antibiotics and Antibiotic-Resistant Bacteria," *Chemical Engineering Journal* 498 (2024): 155740, https://doi.org/10.1016/j.cej.2024.155740.

94. C. Shang, Y. Chen, Z. Dai, et al., "Nanotechnology-Enabled Devices for Ocean Internet of Things," *EcoMat* 7, no. 3 (2025): e70003, https://doi.org/10.1002/eom2.70003.

95. Y. Zhang, Y. Ma, L. Wang, Q. Sun, F. Zhang, and J. Shi, "Facile One-Step Hydrothermal Synthesis of Noble-Metal-Free Hetero-Structural Ternary Composites and Their Application in Photocatalytic Water Purification," *RSC Advances* 7, no. 80 (2017): 50701–50712, https://doi.org/10.1039/C7RA10732C.

96. L. Sun, L. Xiang, X. Zhao, et al., "Enhanced Visible-Light Photocatalytic Activity of BiOI/BiOCl Heterojunctions: Key Role of Crystal Facet Combination," *ACS Catalysis* 5, no. 6 (2015): 3540–3551, https://doi.org/10.1021/cs501631n.

97. P. Chen, H. Liu, W. Cui, S. C. Lee, L. a. Wang, and F. Dong, "Bi-Based Photocatalysts for Light-Driven Environmental and Energy Applications: Structural Tuning, Reaction Mechanisms, and Challenges," *EcoMat* 2, no. 3 (2020): e12047, https://doi.org/10.1002/eom2.12047.

98. Z. Zhou, Z. Shen, Z. Cheng, et al., "Mechanistic Insights for Efficient Inactivation of Antibiotic Resistance Genes: A Synergistic Interfacial Adsorption and Photocatalytic-Oxidation Process," *Science Bulletin (Beijing)* 65, no. 24 (2020): 2107–2119, https://doi.org/10.1016/j.scib.2020.07.015.

99. B. Li and T. Yan, "Next Generation Sequencing Reveals Limitation of qPCR Methods in Quantifying Emerging Antibiotic Resistance Genes (ARGs) in the Environment," *Applied Microbiology and Biotechnology* 105, no. 7 (2021): 2925–2936, https://doi.org/10.1007/s00253-021-11202-4.

100. Z. Ren, B. Yang, E. Petropoulos, et al., "Under What Circumstances Can Chemical Oxidation Processes Effectively Degrade Antibiotics Resistance Genes? Evidence From Meta-Analysis," *Journal of Environmental Chemical Engineering* 12, no. 5 (2024): 113385, https://doi.org/10.1016/j.jece.2024.113385.

101. X. Zhang, J. Li, W.-Y. Fan, M.-C. Yao, L. Yuan, and G.-P. Sheng, "Enhanced Photodegradation of Extracellular Antibiotic Resistance Genes by Dissolved Organic Matter Photosensitization," *Environmental Science & Technology* 53, no. 18 (2019): 10732–10740, https://doi.org/10.1021/acs.est.9b03096.

102. S. Garg and T. D. Waite, "Is Singlet Oxygen an Important Oxidant in Advanced Oxidation Processes?," *Environmental Science & Technology* 59, no. 49 (2025): 26320–26341, https://doi.org/10.1021/acs.est.5c09597.

103. J. Peng, Y. Pan, Y. Zhou, et al., "Triplet Photochemistry of Effluent Organic Matter in Degradation of Extracellular Antibiotic Resistance Genes," *Environmental Science & Technology* 57, no. 18 (2023): 7230–7239, https://doi.org/10.1021/acs.est.2c08036.

104. J. Cai, B. Niu, Q. Xie, et al., "Accurate Removal of Toxic Organic Pollutants From Complex Water Matrices," *Environmental Science & Technology* 56, no. 5 (2022): 2917–2935, https://doi.org/10.1021/acs.est.1c07824.

105. S. He, Z. Hu, C. He, et al., "Nanoconfinement-Enabled Resistance to Water Matrix Components for Selective Degradation of Micropollutants," *Angewandte Chemie International Edition* 64, no. 14 (2025): e202424827, https://doi.org/10.1002/anie.202424827.

106. W. Yin, T. Liu, J. Chen, et al., "Using UV/Peracetic Acid as Pretreatment for Subsequent Bio-Treatment of Antibiotic-Containing Wastewater Treatment: Mitigating Microbial Inhibition and Antibiotic Resistance Genes Proliferation," *Journal of Hazardous Materials* 470 (2024): 134166, https://doi.org/10.1016/j.jhazmat.2024.134166.

107. P. La Manna, M. De Carluccio, G. Oliva, G. Vigliotta, and L. Rizzo, "Urban Wastewater Disinfection by Iron Chelates Mediated Solar Photo-Fenton: Effects on Seven Pathogens and Antibiotic Resistance Transfer Potential," *Water Research* 249 (2024): 120966, https://doi.org/10.1016/j.watres.2023.120966.

108. J. Bockenstedt, N. A. Vidwans, T. Gentry, and S. Vaddiraju, "Catalyst Recovery, Regeneration and Reuse During Large-Scale Disinfection of Water Using Photocatalysis," *Water* 13, no. 19 (2021): 2623.

109. C. González-Fernández, E. Bringas, M. J. Rivero, and I. Ortiz, "Revealing the Role of Magnetic Materials in Light-Driven Advanced Oxidation Processes: Enhanced Degradation of Contaminants and Facilitated Magnetic Recovery," *Frontiers in Chemical Engineering* 6 (2024): 1430773, https://doi.org/10.3389/fceng.2024.1430773.

110. J. Hou, Y. Fan, Z. Yang, et al., "Advancements in Water Purification: A Defective MPN-Based Light-Responsive Self-Cleaning Membrane for Superior Bacteria and Resistance Gene Removal, Biofouling Mitigation, and Mechanistic Insights," *Journal of Environmental Chemical Engineering* 12, no. 3 (2024): 113060, https://doi.org/10.1016/j.jece.2024.113060.

111. S. Ren, C. Boo, N. Guo, S. Wang, M. Elimelech, and Y. Wang, "Photocatalytic Reactive Ultrafiltration Membrane for Removal of Antibiotic Resistant Bacteria and Antibiotic Resistance Genes From Wastewater Effluent," *Environmental Science and Technology* 52, no. 15 (2018): 8666–8673, https://doi.org/10.1021/acs.est.8b01888.

112. R. Li, Z. Wei, P. Li, et al., "Novel Visible-Light Activated Photocatalytic Ultrafiltration Membrane for Simultaneous Separation and Degradation of Emerging Contaminants," *Journal of Hazardous Materials* 478 (2024): 135634, https://doi.org/10.1016/j.jhazmat.2024.135634.

113. R. Hischier and T. Walser, "Life Cycle Assessment of Engineered Nanomaterials: State of the Art and Strategies to Overcome Existing Gaps," *Science of the Total Environment* 425 (2012): 271–282, https://doi.org/10.1016/j.scitotenv.2012.03.001.

114. L. M. d. Luz, A. C. d. Francisco, C. M. Piekarski, and R. Salvador, "Integrating Life Cycle Assessment in the Product Development Process: A Methodological Approach," *Journal of Cleaner Production* 193 (2018): 28–42, https://doi.org/10.1016/j.jclepro.2018.05.022.

115. S. Fernandes, J. C. G. Esteves da Silva, and L. Pinto da Silva, "Life Cycle Assessment of the Sustainability of Enhancing the Photodegradation Activity of TiO_2 With Metal-Doping," *Materials* 13 (2020): 1487.

116. N. Aquino de Carvalho and L. M. Gilbertson, "Comparative Life Cycle Assessment of Graphitic Carbon Nitride Synthesis Routes," *Journal of Industrial Ecology* 27, no. 3 (2023): 1008–1020, https://doi.org/10.1111/jiec.13390.

117. A. Rezaie, E. khaki, H. Boleydei, B. Khoshnevisan, and S. Fayyaz, "Environmental, Energy and Economic Assessment of Four Recyclable Nano-Sized Semiconductor Photocatalysts to Remove 2,4-Dichlorophenol," *Journal of Water Process Engineering* 77 (2025): 108351, https://doi.org/10.1016/j.jwpe.2025.108351.

118. T. Lakshmi, S. S. Priya, L. Mulky, K. Sudhakar, and M. Tahir, "A Comprehensive Review on N-Metallic Photocatalysts and Photoreactor Designs for Enhanced Photocatalytic Reduction of Carbon Dioxide to Value-Added Fuels," *Chemical Engineering Journal* 520 (2025): 165751, https://doi.org/10.1016/j.cej.2025.165751.

119. H. Sudrajat and M. Nobatova, "Heterojunction Photocatalysts: Where Are They Headed?," *RSC Applied Interfaces* 2, no. 3 (2025): 599–619, https://doi.org/10.1039/d5lf00037h.

120. Y. Xie, T. Zhang, H. Guo, et al., "Decatungstate-Driven Photocatalytic Pathways for Sustainable and Cleaner Recovery of Precious Metals," *Angewandte Chemie International Edition* 64, no. 24 (2025): e202505651, https://doi.org/10.1002/anie.202505651.

121. Y. Chen, M. Xu, J. Wen, et al., "Selective Recovery of Precious Metals Through Photocatalysis," *Nature Sustainability* 4, no. 7 (2021): 618–626, https://doi.org/10.1038/s41893-021-00697-4.

122. J. J. Zhang, Y. F. Song, Y. Liu, X. M. Tian, and R. X. Gao, "Fabrication of High-Degradation-Efficiency Molecularly Imprinted Photocatalysts and Its Selective Degradation Performance," *Se Pu* 44, no. 1 (2026): 78–91, https://doi.org/10.3724/sp.J.1123.2025.06001.

123. J. Shin, S. R. Kim, Z. Xie, Y. S. Jin, and Y. C. Wang, "A CRISPR/Cas12a-Based System for Sensitive Detection of Antimicrobial-Resistant Genes in Carbapenem-Resistant Enterobacterales," *Biosensors-Basel* 14, no. 4 (2024): 194, https://doi.org/10.3390/bios14040194.

124. X. Li, N. Bao, Z. Yan, X. Z. Yuan, S. G. Wang, and P. F. Xia, "Degradation of Antibiotic Resistance Genes by VADER With CRISPR-Cas Immunity," *Applied and Environmental Microbiology* 89, no. 4 (2023): e0005323, https://doi.org/10.1128/aem.00053-23.

125. A. Mukarram, A. Zain Ul, M. Muhammad, M. Saeed, H. Sharafat, and Z. Ali, "Dual Action Approach of Nano Particles and CRISPR/

CAS-9 to Overcome Antibiotic Resistance; A Systematic Review," *Insights-Journal of Health and Rehabilitation* 3 (2025): 917–924, https://doi.org/10.71000/915se539.

126. A. Saffari Natanzi, M. Poudineh, E. Karimi, A. Khaledi, and H. Haddad Kashani, "Innovative Approaches to Combat Antibiotic Resistance: Integrating CRISPR/Cas9 and Nanoparticles Against Biofilm-Driven Infections," *BMC Medicine* 23, no. 1 (2025): 486, https://doi.org/10.1186/s12916-025-04323-4.

127. P. Prieto-Laria, A. Jiménez-Rodríguez, A. R. Ruiz-Salvador, et al., "From the Lab to the River: Bimetallic Clinoptilolite Photocatalyst for Antibiotic-Resistant Bacteria and Emerging Contaminants Removal," *Journal of Environmental Chemical Engineering* 13, no. 3 (2025): 116663, https://doi.org/10.1016/j.jece.2025.116663.

128. L. Liu, C. Liu, J. Zheng, et al., "Elimination of Veterinary Antibiotics and Antibiotic Resistance Genes From Swine Wastewater in the Vertical Flow Constructed Wetlands," *Chemosphere* 91, no. 8 (2013): 1088–1093, https://doi.org/10.1016/j.chemosphere.2013.01.007.

129. P. Chen, X. Yu, and J. Zhang, "Photocatalysis Enhanced Constructed Wetlands Effectively Remove Antibiotic Resistance Genes From Domestic Wastewater," *Chemosphere* 325 (2023): 138330, https://doi.org/10.1016/j.chemosphere.2023.138330.

130. H. Masood, C. Y. Toe, W. Y. Teoh, V. Sethu, and R. Amal, "Machine Learning for Accelerated Discovery of Solar Photocatalysts," *ACS Catalysis* 9, no. 12 (2019): 11774–11787, https://doi.org/10.1021/acscatal.9b02531.

131. H. Masood, T. Sirojan, C. Y. Toe, et al., "Enhancing Prediction Accuracy of Physical Band Gaps in Semiconductor Materials," *Cell Reports Physical Science* 4, no. 9 (2023): 101555, https://doi.org/10.1016/j.xcrp.2023.101555.

132. J. Y. Y. Loh, A. Wang, A. Mohan, et al., "Leave No Photon Behind: Artificial Intelligence in Multiscale Physics of Photocatalyst and Photoreactor Design," *Advanced Science* 11, no. 18 (2024): 2306604, https://doi.org/10.1002/advs.202306604.

133. Z. Jiang, J. Hu, M. Tong, A. C. Samia, H. Zhang, and X. Yu, "A Novel Machine Learning Model to Predict the Photo-Degradation Performance of Different Photocatalysts on a Variety of Water Contaminants," *Catalysts* 11 (2021): 1107.

134. H. Ni, H. Liu, Y. Zhang, X. Yang, and Y. Shen, "High-Throughput Discovery of Surface-Functionalized MXenes for Photocatalytic Water Splitting via Integrated Machine Learning and DFT Screening," *Applied Physics Letters* 127, no. 11 (2025): 113906, https://doi.org/10.1063/5.0288263.

135. D. Ontiveros, S. Vela, F. Viñes, and C. Sousa, "MXgap: A MXene Learning Tool for Bandgap Prediction," *ACS Catalysis* 15, no. 16 (2025): 14403–14413, https://doi.org/10.1021/acscatal.5c04191.

136. Z. Jiang, J. Hu, A. Samia, and X. Yu, "Predicting Active Sites in Photocatalytic Degradation Process Using an Interpretable Molecular-Image Combined Convolutional Neural Network," *Catalysts* 12 (2022): 746.

137. A. Dubey, S. L. Sanchez, J. Yang, and M. Ahmadi, "Lead-Free Halide Perovskites for Photocatalysis via High-Throughput Exploration," *Chemistry of Materials* 36, no. 5 (2024): 2165–2176, https://doi.org/10.1021/acs.chemmater.3c03186.